①

THIRD & FOURTH QUARTER PROGRESS
REPORT 1987 ON PLASMA THEORY
AND SIMULATION

## DTIC
S ELECTE
SEP 2 7 1988
D

AD-A199 454

July 1 to December 31, 1987

88 9 26 094

# ELECTRONICS RESEARCH LABORATORY
## College of Engineering
## University of California, Berkeley, CA 94720

| REPORT DOCUMENTATION PAGE | | READ INSTRUCTIONS BEFORE COMPLETING FORM |
|---|---|---|
| 1. REPORT NUMBER | 2. GOVT ACCESSION NO. | 3. RECIPIENT'S CATALOG NUMBER |
| 4. TITLE (and Subtitle) Quarterly Progress Report, III, IV July 1, 1987 - December 31, 1987 | | 5. TYPE OF REPORT & PERIOD COVERED Progress, 7/1-12/31, 1987 |
| | | 6. PERFORMING ORG. REPORT NUMBER |
| 7. AUTHOR(s) Professor Charles K. Birdsall | | 8. CONTRACT OR GRANT NUMBER(s) ONR N00014-85-K-0809 |
| 9. PERFORMING ORGANIZATION NAME AND ADDRESS Electronics Research Laboratory University of California Berkeley, CA 94720 | | 10. PROGRAM ELEMENT, PROJECT, TASK AREA & WORK UNIT NUMBERS Element No. 61153N, Project Task Area RR01-09-01, Work Unit No. NR 012-742 |
| 11. CONTROLLING OFFICE NAME AND ADDRESS ONR Physics Division Department of the Navy, ONR Arlington, VA 22217 | | 12. REPORT DATE |
| | | 13. NUMBER OF PAGES |
| 14. MONITORING AGENCY NAME & ADDRESS(If different from Controlling Office) | | 15. SECURITY CLASS. (of this report) Unclassified |
| | | 15a. DECLASSIFICATION/DOWNGRADING SCHEDULE |

16. DISTRIBUTION STATEMENT (of this Report)

Approved for public release; distribution unlimited

17. DISTRIBUTION STATEMENT (of the abstract entered in Block 20, If different from Report)

18. SUPPLEMENTARY NOTES
Our group uses theory and simulation as tools in order to increase the understanding of plasma instabilities, heating, transport, plasma-wall interactions, and large potentials in plasmas. We also work on the improvement of simulation both theoretically and practically.

19. KEY WORDS (Continue on reverse side if necessary and identify by block number)

Research in plasma theory and simulation, plasma-wall interactions, large potentials in plasmas.

20. ABSTRACT (Continue on reverse side if necessary and identify by block number)

See reverse side

DD FORM 1473 1 JAN 73     EDITION OF 1 NOV 65 IS OBSOLETE
S/N 0102-LF-014-6601

## 20. ABSTRACT

### General Plasma Theory and Simulation '

A. A magnetized plasma next to an absorbing wall is simulated, showing positive wall charging causing a large E-field near the wall, then a large E×B drift, then a Kelvin-Helmholtz instability, vortices and coalescence. Particle transport to the walls is Bohm-like, for $\omega_{pi} > 2\omega_{ci}$.

B. A kinetic theory, allowing finite ion Larmor radii, general magnetic field geometries and plasma equilibria, has been developed for hydromagnetic Alfvén waves excited within the Earth's magnetosphere by the storm-time energetic ring-current particles.

### Plasma Wall Physics, Theory and Simulation

A. Multi-time and space scaling for bounded plasmas is being developed using an implicit method.

B. It is found that using large time steps, $\omega_{ce}\Delta t > 1$ provides reliable guiding center motions for single particles.

C. Electron-neutral elastic scattering is added to ES1 readily. Runs with initial beam verify predictions.

D. RF heating (ECRH) is shown to work well with PIC simulations, providing results very similar to a Monte Carlo RF heating code.

# THIRD AND FOURTH QUARTER PROGRESS REPORT
## ON
## PLASMA THEORY AND SIMULATION

### July 1 to December 31, 1987

Our research group uses both theory and simulation as tools in order to increase the understanding of instabilities, heating, transport, plasma-wall interactions, and large potentials in plasmas. We also work on the improvement of simulation, both theoretically and practically.

**Our staff is:**

| | | | |
|---|---|---|---|
| Professor C.K. Birdsall<br>*Principal Investigator* | 191M | Cory Hall | 643-6631 |
| Dr. Kim Theilhaber<br>*Post-doctorate* | 187M | Cory Hall | 642-3477 |
| Mr. William Lawson | 199MD | Cory Hall | 642-1297 |
| Mr. Scott Parker | 199MD | Cory Hall | 642-1297 |
| Mr. Richard Procassini | 199MD | Cory Hall | 642-1297 |
| Ms. Lou Ann Schwager | 199MD | Cory Hall | 642-1297 |
| Ms. Julia Little<br>*Research Assistants(students)* | 199MD | Cory Hall | 642-1297 |

**Our advisers and Associates are:**

| | | | |
|---|---|---|---|
| Dr. Illan Roth<br>*Physicist, Space Science Lab, UCB* | 304 | SSL | 642-1327 |
| Dr. Bruce Cohen | L630 | LLNL | 422-9823 |
| Dr. Alex Friedman | L630 | LLNL | 422-0827 |
| Dr. A. Bruce Langdon<br>*Physicists, Lawrence Livermore Natl. Lab* | L472 | LLNL | 422-5444 |

December 31,1987

ELECTRONICS RESEARCH LABORATORY
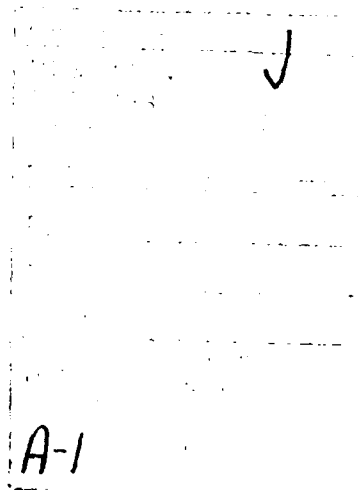
University of California
Berkeley, CA 94720

A-1

-i-

# Table of Contents

# SECTION I: GENERAL PLASMA THEORY AND SIMULATION

**A. Vortex formation and particle transport in a cross-field plasma sheath**
*K. Theilhaber*

## Abstract

The time-dependent behavior of a transversely magnetized, two-dimensional plasma-wall sheath has been studied through particle simulations, with the aim of modelling plasma behavior in the vicinity of the limiters and walls of magnetized plasma devices. The simulations have shown that the cross-field sheath between a wall and a plasma is a turbulent boundary layer, with strong potential fluctuations and anomalous particle transport. The driving mechanism for this turbulence is the Kelvin-Helmholtz instability, which arises from the sheared particle drifts created near the wall. Provided it is replenished by an internal flux of particles, the sheath maintains itself in a dynamic equilibrium, in which the linear edge instability, the nonlinear dynamics of the particles and the outward particle diffusion all balance each other. The sheath assumes an equilibrium thickness of order $l_x \sim 5\,\rho_i$, and maintains large, long-lived vortices, with amplitudes $\delta\phi \sim 2T_i/e$, which drift parallel to the wall at roughly half the ion thermal velocity. The sheath also maintains a large, spatially-averaged potential drop from the wall to the plasma, with $\Delta\phi \approx -1.5T_i/e$, in sharp distinction with the unmagnetized sheath, where the plasma potential is *higher* than at the wall. Accompanying the long-wavelength vortices is a spectrum of shorter-wavelength fluctuations, which extend to $|k|\,\rho_i \sim 1$ and $\omega \sim \omega_{ci}$, and which induce an anomalous cross-field transport. A central result is that the anomalous transport scales like Bohm diffusion, at least when $\omega_{pi} \geq 2\omega_{ci}$. At lower densities, $\omega_{pi} < 2\omega_{ci}$, the diffusion coefficient has an additional factor, proportional to the density. These results enable us to model the cross-field sheath by a simple boundary condition, which relates the particle flux through the sheath to the edge density and which can be used as input in any model designed to obtain the bulk plasma properties.

# B. On Magnetospheric Hydromagnetic Waves Excited by Energetic Ring-Current Particles

*Liu Chen*[*]
Department of Electrical Engineering and Computer Sciences,
University of California at Berkeley, Berkeley, Calif. 94720

and

*Akira Hasegawa*
AT&T Bell Laboratories
Murray Hill, New Jersey 07974

*Abstract.* A kinetic theory, allowing finite ion Larmor radii, general magnetic field geometries and plasma equilibria, has been developed for hydromagnetic Alfven waves excited within the Earth's magnetosphere by the storm-time energetic ring-current particles. In particular, assuming adiabatically injected particles, it is found that the excitation mechanism is due to the magnetic drift-bounce resonances of highly energetic protons and the various predicted instability properties are consistent with satellite observations.

---

[*] Permanent address: Plasma Physics Laboratory, Princeton University, Princeton. N.J. 08544

# INTRODUCTION

Recent multiple-satellite observations [Takahashi et al., 1985] of dayside compressional Pc5 pulsations have stimulated renewed theoretical interest in the excitation mechanisms of magnetospheric hydromagnetic waves during geomagnetic storms. Briefly stated, the observations have the following properties: (1) occurrences mostly during the recovery phases of geomagnetic storms, (2) large azimuthal (East-West) wave numbers; typically, $m \sim O(10^2)$, (3) westward phase velocities similar to the ion magnetic drift velocities, and (4) frequencies roughly corresponding to those of standing shear Alfvén waves. Properties similar to (2), (3), and (4) were also observed in storm-time Pc5 pulsations by STARE radar [Allan et al., 1982]. In one event, antisymmetric structures along the magnetic field lines were also identified [Takahashi and Higbie, 1986; Takahashi et al., 1987].

Since $\beta$ ($\beta \equiv$ plasma pressure/magnetic pressure) values are typically low, $\beta \sim O(0.3)$, during the recovery phases, these observations appear to indicate that the drift-mirror instability mechanism, as originally proposed by Hasegawa [1969], and its variations [Walker et al., 1982; Pokhotelov et al., 1986] may be inadequate in explaining these events. On the other hand, excitations via wave-particle resonances remain viable even at low $\beta$ values. Previous theoretical investigations in this direction are, however, limited to either local WKB ansatz (i.e., neglecting eigenmode field-aligned structures) [Meerson et al., 1978] or the long-wavelength drift-kinetic approximation [Southwood, 1976]. Since $m \sim O(10^2) \gg 1$, the drift-kinetic approximation, which assumes

-3-

$|k_\perp \rho| < 1$ ($k_\perp$ and $\rho$ being, respectively, the wave number perpendicular to **B** and the Larmor radius) becomes, strictly speaking, invalid for highly energetic protons. Furthermore, the $|k_\perp \rho| < 1$ approximation also implies that the magnetic drift frequencies are much smaller than the bounce frequencies and, hence, precludes the potentially important wave-particle interactions via magnetic drift-bounce resonances [Southwood, 1976]. In the present work, we reexamine this subject employing the more consistent gyrokinetic equations [Antonsen and Lane, 1980; Catto, et al., 1981], which includes effects of finite ion Larmor radii, general magnetic field geometries, and plasma equilibria as well as field-aligned eigenmode structures. In order to isolate the responsible physical mechanisms, we shall ignore pressure anisotropy (i.e., the drift-mirror mode) and concentrate on instabilities excited via wave-particle interactions.

## THEORETICAL FORMULATION AND GYROKINETIC EQUATIONS

To include finite ion Larmor radius effects in the formulation of low-frequency hydromagnetic waves, we adopt the following gyrokinetic orderings $\omega/\Omega \sim k_\parallel \rho \sim k_\parallel/k_\perp \sim \rho/L_o \ll 1$. and $k_\perp \rho \sim O(1)$; where $\Omega$ and $\rho$ are, respectively, cyclotron frequency and radius, and $L_o$ is the equilibrium scale length. Thus, within these orderings, the parallel wave length is $O(L_o)$, and one must retain the parallel eigenmode structures. Meanwhile, the linearized Vlasov equation can be reduced by first transforming to the guiding-center phase space $[\mathbf{X} = \mathbf{x} + \mathbf{v} \times e_\parallel/\Omega, \mathbf{V} = (\epsilon = v^2/2, \mu = v_\perp^2/2B, \alpha = \text{gyrophase angle})]$ and then averaging over the fast-varying gyrophase $\alpha$. Here, $e_\parallel = \mathbf{B}/B$. Assuming WKB ansatz for the variations perpendicular to **B**, i.e., $\delta f(\mathbf{x}, \mathbf{v}, t) =$

$\delta\hat{f}(\ell, \mathbf{v})\exp[i\int^{x_1}(\mathbf{k}_\perp\cdot d\mathbf{x}_\perp - i\omega t)$ with $\ell$ being the coordinate along $\mathbf{B}$. we then have, for isotropic plasmas considered here,

$$\delta\hat{f} = (q/m)[\delta\hat{\phi}\frac{\partial F_o}{\partial\epsilon} - J_o(\lambda)\delta\hat{\psi}e^{iL_k}(\frac{Q}{\omega})F_o] + \delta\hat{g}e^{iL_k}, \qquad (1)$$

$$QF_o = (\omega\partial/\partial\epsilon + \hat{\omega}_*)F_o, \qquad (2)$$

$\hat{\omega}_*F_o = (\mathbf{k}\times\mathbf{e}_{\parallel}/\Omega)\cdot\nabla F_o$, $\lambda = k_\perp\rho$, $L_k = \mathbf{k}_\perp\cdot\mathbf{e}_{\parallel}\times\mathbf{v}/\Omega$ corresponds to finite Larmor-radius effect via transformation between $\mathbf{x}$ and $\mathbf{X}$, and the field variables are $\delta\hat{\phi}$, $c\partial\delta\hat{\psi}/\partial\ell = i\omega\delta\hat{A}_{\parallel}$, and $\delta\hat{B}_{\parallel}$. Meanwhile. $\delta\hat{g}$, satisfies the following linearized gyrokinetic equation

$$[v_{\parallel}\frac{\partial}{\partial\ell} - i(\omega - \omega_d)]\delta\hat{g} = i\frac{q}{m}QF_o\delta\hat{S}, \qquad (3)$$

where

$$\delta\hat{S} = J_o(\delta\hat{\phi} - \delta\hat{\psi}) + J_o\omega_d\delta\hat{\psi}/\omega + J_1 v_\perp\delta\hat{B}_{\parallel}/k_\perp c, \qquad (4)$$

$\omega_d = \mathbf{k}_\perp\cdot\mathbf{v}_d$, and $\mathbf{v}_d$ is the magnetic drift velocity given by $\mathbf{v}_d = \mathbf{e}_{\parallel}\times[(v_\perp^2/2)\nabla\ln B + v_{\parallel}^2\kappa]/\Omega$ with $\kappa = (\mathbf{e}_{\parallel}\cdot\nabla)\mathbf{e}_{\parallel}$ being the curvature. Given particles are magnetically trapped between $\ell_1$ and $\ell_2$, Eq. (3) can be readily solved. In particular, one finds

$$\delta\hat{G} \equiv \frac{1}{2}\sum_\sigma\delta\hat{g}(\sigma) = -(\frac{q}{m})QF_o\{\cot I_{\ell_1}^{\ell_2}\cos I_{\ell_1}^{\ell}\tau_b\overline{\delta\hat{S}\cos I_{\ell_1}^{\ell}}$$

$$+ \cos I_{\ell_1}^{\ell}\tau_b\overline{\delta\hat{S}\sin I_{\ell_1}^{\ell}} + \int_{\ell_1}^{\ell}\frac{d\hat{\ell}}{|v_{\parallel}|}\delta\hat{S}\sin I_{\hat{\ell}}^{\ell}\}, \qquad (5)$$

where $\sigma = \text{sgn}(v_{\parallel})$, $I_a^b = \int_a^b d\ell(\omega - \omega_d)/|v_{\parallel}|$, $\tau_b = \int_{\ell_1}^{\ell_2}d\ell/|v_{\parallel}|$ and $\overline{A} \equiv [\int_{\ell_1}^{\ell_2}Ad\ell/|v_{\parallel}|]/\tau_b$. Note that $\cot I_{\ell_1}^{\ell_2} = \sum_{K=-\infty}^{\infty}(\omega - \bar{\omega}_d - K\omega_b)^{-1}/\tau_b$, where

-5-

$\omega_b = \pi/\tau_b$. Equation (5), thus, contains wave-particle interactions via the magnetic drift and bounce resonances.

For hydromagnetic waves, the relevant field equations are the quasi-neutrality condition and the Ampere's law. Specifically, the quasi-neutrality condition yields

$$\sum_j (q^2/m)_j < \delta\hat{\varphi}\frac{\partial F_o}{\partial\epsilon} - (\frac{Q}{\omega})F_o\delta\psi J_o^2 + (\frac{m}{q})J_o\delta\hat{G} >_j = 0, \qquad (6)$$

with $j =$ species and $<...> \equiv 4\pi \int (...) \, Bd\mu d\epsilon/|v_{||}|$. The perpendicular Ampere's law gives

$$\delta\hat{B}_{||} = \frac{4\pi}{ck_\perp}\sum_j < qv_\perp J_1(\frac{q}{m}\frac{Q}{\omega}F_oJ_o\delta\hat{\psi} - \delta\hat{G}) >_j. \qquad (7)$$

Meanwhile, the parallel Ampere's law when combined with the quasi-neutrality condition yields the following generalized vorticity equation

$$\frac{1}{4\pi}\frac{c^2}{\omega^2}B\frac{\partial}{\partial\ell}\frac{k_\perp^2}{B}\frac{\partial}{\partial\ell}\delta\hat{v} = \sum_j q_j < \frac{\omega_d}{\omega}J_o\delta\hat{G} + \frac{q}{m}[\delta\hat{\varphi}\frac{\partial F_o}{\partial\epsilon}$$
$$- \frac{Q}{\omega}F_o(J_o^2\delta\hat{\varphi} + J_o^2\frac{\omega_d}{\omega}\delta\hat{\psi} + J_oJ_1\frac{v_\perp}{k_\perp c}\delta\hat{B}_{||})] >_j. \qquad (8)$$

Equations (6) to (8) along with $\delta\hat{G}$ given by Eq. (5) form the complete set of equations, which, however, generally requires numerical solutions. Subsidiary expansions are needed in order to make analytical progress and they are carried out in the next section.

# EIGENMODE EQUATIONS AND GENERAL STABILITY PROPERTIES

Consistent with observations at the geosynchronous orbit, the ring-current plasma of electrons and, mainly, protons is taken to consist of core (c), warm (w), and hot (h) components. The corresponding temperatures are, formally, $T_c \sim O(1)$ keV, $T_w \sim O(10)$ keV, and $T_h \sim O(10^2)$ keV. Thus, $T_c/T_w \sim T_w/T_h \sim 10^{-1} \equiv \delta^2$ and $\delta$ is the smallness parameter for the subsidiary expansions. Meanwhile, we have $n \sim O(10/cm^3$), which takes into account the presence of heavy elements and $B \sim O(10^2)\gamma$. In terms of $\delta$, we also assume, for recovery phases, $\beta_c \sim \beta_w \sim \delta$ and $\beta_h \sim \delta^2$, which implies $n_w/n_c \sim \delta^2$ and $n_h/h_c \sim \delta^5$. As to frequency and wavelength orderings, we assume $\omega \sim O(V_A/L_o)$, $k_{\parallel}L_o \sim O(1)$, and $m \sim O(10^2)$. We, therefore, have $k_\perp \rho_{ih} \sim O(1)$, $k_\perp \rho_{iw} \sim O(\delta)$, $k_\perp \rho_{ic} \sim O(\delta^2)$, and $k_\perp \rho_e$ being negligible. In addition, we have $\omega_{dc}/\omega \sim \omega_{*c}/\omega \sim \delta^{5/2}$; $\omega_{dw}/\omega \sim \omega_{*w}/\omega \sim \delta^{1/2}$; $\omega_{dh}/\omega \sim \omega_{*h}/\omega \sim \delta^{-3/2}$; with $\omega_* \sim \epsilon \hat{\omega}_*$ being the typical diamagnetic drift frequency, and $\omega_{b,ic}/\omega \sim \delta^{1/2}$, $\omega_{b,iw}/\omega \sim \delta^{-1/2}$, $\omega_{b,ih}/\omega \sim \delta^{-3/2}$ as well as $\omega/\omega_{b,e}$ being negligible. Briefly stated, the physical significance of the above orderings are (i) while the core component supports the hydromagnetic waves, the warm and hot component provide the instability-driving finite-$\beta$ effects, (ii) while the core ions respond to local perturbations, the rest of the components mainly respond to bounce-averaged perturbations, (iii) for electrons, only the warm component experiences wave-particle interactions via the magnetic drift resonances, (iv) for ions, however, while the wave component experiences both the magnetic drift and the bounce resonances, the hot component experiences magnetic drift-bounce

resonances, and, finally, (v) only the finite Larmor-radius effects of hot ions need to be kept.

Application of the above orderings further simplifies the set of equations derived in the preceding section. Specifically, to the lowest order of accuracy, Eq. (6), the quasi-neutrality condition, reduces to

$$< \frac{\partial F_0}{\partial \epsilon} (\delta \hat{\xi} - \overline{\delta \xi})>_e = < \frac{\partial F_0}{\partial \epsilon} (\overline{\omega_d \delta \hat{\varphi}} - \omega_d \delta \hat{\varphi})>_e , \qquad (9)$$

where $\delta \hat{\xi} \equiv \omega(\delta \hat{\varphi} - \delta \hat{w})$ and is, thus, proportional to the parallel electric field, $\delta E_{\parallel}$. Equation (9) indicates that in realistic magnetic field geometries, $\delta E_{\parallel}$ could be generated via magnetic drifts. Equation (7), the perpendicular Ampere's law, meanwhile, becomes

$$\frac{\delta \hat{B}_{\parallel}}{B} = \frac{4\pi}{\omega B^2} \{ n_i q_i (\omega_{*,ti}, -\omega_{*,te} - 3\omega_{\kappa,ti}) \delta \hat{\varphi}$$

$$+ q_e < \frac{\partial F_0}{\partial \epsilon} \frac{v_{\perp}^2}{2} (\overline{\omega_d \delta \hat{\varphi}} + \overline{\delta \hat{\xi}} - \delta \hat{\xi})>_e + q_i < \frac{\partial F_0}{\partial \epsilon} \frac{v_{\perp}^2}{2} \overline{\omega_d \delta \hat{\varphi}}>_{iw} \} . \qquad (10)$$

where $n_j \omega_{*,tj} = <(v_{\perp}^2/2) \hat{\omega}_* F_0>_j$, $n_j \omega_{\kappa,tj} = <(v_{\perp}^2/2)\hat{\omega}_\kappa F_0>_j$, and $\hat{\omega}_{\kappa j} = (e_{\parallel} \times \kappa) \cdot k/\Omega_j$. Note that Eq. (10) corresponds to the magnetostatic approximation, i.e., $B\delta B_{\parallel} + 4\pi \delta P_{\perp} \simeq 0$. Finally, the generalized vorticity equation becomes

$$B\frac{\partial}{\partial \ell}\frac{k_\perp^2}{B}\frac{\partial}{\partial \ell}\delta\hat{\phi} + \frac{\omega^2 k_\perp^2}{V_A^2}\delta\hat{\phi} = -\frac{8\pi n_i e^2}{m_i c^2}\hat{\omega}_{\kappa i}(\omega_{*,ti} - \omega_{*,te})\delta\hat{\phi}$$

$$-\frac{4\pi e^2}{m_i c^2} < \frac{\partial F_o}{\partial \epsilon}\omega_d^2 \delta\hat{\phi} >_{ic} - \frac{4\pi}{c^2}\sum_{j=e,iw}(\frac{q^2}{m})_j < \frac{\partial F_o}{\partial \epsilon}\omega_d\overline{\omega_d\delta\hat{\phi}} >_j$$

$$+\frac{4\pi e^2}{m_e c^2} < \frac{\partial F_o}{\partial \epsilon}\omega_d\delta\hat{\xi} >_e$$

$$+ i\frac{4\pi^2}{c^2}\sum_{j=e,i}(\frac{q^2}{m})_j < QF_o\sum_K \delta(\omega-\overline{\omega}_d-K\omega_b)\omega_d J_o\cos I_{\ell_1}^\ell \overline{J_o\omega_d \delta\hat{\phi}\cos I_{\ell_1}^\ell}. \quad (11)$$

Here, we note that $\delta\hat{B}_\parallel$ does not appear due to the low-$\beta$ ordering, $\beta \sim \delta$, and that $\delta\hat{\xi}$ is related of $\delta\hat{\phi}$ via Eq. (9). Equations (9) to (11), thus, represent a set of reduced equations more susceptible to analytical and numerical treatments.

Some interesting insights to the general stability properties can, however, be obtained from the quadratic forms readily derivable from Eqs. (9) and (11). Denoting $||a|| \equiv \oint_{\ell_S}^{\ell_N} a\, d\ell/B$ with $\ell_S$ and $\ell_N$ being the end points of the field line and $\delta\hat{\phi}(\ell = \ell_S, \ell_N) = 0$, we have, for $\omega^2 \simeq \omega_r^2 + 2i\,\omega_i\omega_r$,

$$\omega_r^2 ||k_\perp^2|\delta\hat{\phi}|^2/V_A^2|| = ||k_\perp^2|\partial\delta\hat{\phi}/\partial\ell|^2|| - R_\beta. \quad (12)$$

$$\omega_i\omega_r = I_\beta/2||k_\perp^2|\delta\hat{\phi}|^2/V_A^2||; \quad (13)$$

where

$$R_\beta = (8\pi n_i e^2/m_i c^2)||\hat{\omega}_{\kappa i}(\hat{\omega}_{*,ti} - \omega_{*,te})|\delta\hat{\phi}|^2||$$

$$+ (16\pi^2/c^2)\int d\mu d\epsilon\{\sum_{j=e,iw}[(q^2/m)(\partial F_o/\partial \epsilon)\tau_b\overline{|\omega_d\delta o|^2}]_j$$

$$+ [(q^2/m)(\partial F_o/\partial \epsilon)\tau_b\omega_d^2\overline{|\delta\hat{\phi}|^2}]_{ic} + [(q^2/m)(\partial F_o/\partial \epsilon)\tau_b(\overline{|\delta\hat{\xi}|^2} - |\overline{\delta\hat{\xi}}|^2)]_e\}.$$

$$(14)$$

and

-9-

$$I_\beta = \frac{16\pi^2}{c^2} \int d\mu d\epsilon \sum_{j=e,i} \sum_K \left[ \frac{q^2}{m} \tau_b QF_o \delta(\omega - \overline{\omega}_d - K\omega_b) \left| \overline{\omega_d J_o \delta\hat{\phi} \cos I^2_{\ell_i}} \right|^2 \right]_j . \quad (15)$$

We now discuss physical meanings of the various terms. For typical cases where $\hat{\omega}_{\kappa i} \omega_{*,ti} > 0$ and $\partial F_o / \partial \epsilon < 0$, the first term in $R_\beta$ corresponds to the bad-curvature interchange/ballooning destabilization, while the second and third terms correspond to stabilization. For $\delta\hat{\phi} =$ constant and balancing these three terms, one can recover the well-known threshold condition on the steepness of the pressure gradients for the interchange stability. On the other hand, noting $\overline{|\delta\xi|^2} - |\overline{\delta\xi}|^2 \geq 0$ from Schwarz' inequality, the last term in $R_\beta$ corresponds to stabilization due to finite electrostatic coupling. Due to the present $\beta \sim 0(\delta) < 1$ ordering, destabilizing (stabilizing) $R_\beta$, i.e., $R_\beta > 0(<0)$, only reduces (increases) $\omega_r$ and has no direct bearing on the stability properties. Extension of the present theory to $\beta \sim 0(1)$ can certainly be conceived and, in such cases, the corresponding Eq. (12) could be expected to play the role of a generalized kinetic energy principle. Thus, in the present work, as we have emphasized earlier and indicated by Eq. (13), stability properties enter only via wave-particle resonances expressed by $I_\beta$ of Eq. (15). To go further with the stability analyses, we need to specify $QF_o$, i.e., both the spatial and velocity dependences of $F_o$. This is carried out in the next section assuming adiabatically injected energetic particles.

## STABILITY OF ADIABATICALLY INJECTED PARTICLES

Noting that, in terms of the longitudinal invariant J, $QF_o$ can be expressed as

$$QF_o = (\omega - \bar{\omega}_d) \frac{\partial F_o}{\partial \epsilon} \Big|_{\mu,L} + (k \times e_\parallel / \Omega) \cdot \nabla L \frac{\partial F_o}{\partial L} \Big|_{\mu,J}. \qquad (16)$$

Here, L, the invariant magnetic latitude, is the equatorial distance of the field line from the symmetry axis. Thus, assuming the energetic ring-current particles are adiabatically injected from the tail such that $\partial F_o / \partial L |_{\mu,J} = 0$, we then have $QF_o = (\omega - \bar{\omega}_d) \partial F_o / \partial \epsilon$, negligible electron contribution $I_{\beta,e} = 0$ since magnetic drift resonances conserves $\mu$ and J, and

$$I_\beta \simeq I_{\beta,i} = \frac{16\pi^2}{c^2} \left( \frac{q^2}{m} \right)_i \int d\mu d\epsilon \left( \frac{\partial F_o}{\partial \epsilon} \right) \sum_K k\pi\delta(\omega_r - \bar{\omega}_d - k\omega_b)$$

$$\times \overline{|\omega_d J_o \cos I_{\ell_i}^\ell \delta\phi|^2}. \qquad (17)$$

At the geosynchronous orbit, where proton pressure, typically, decreases radially outward ($\partial P_i / \partial L < 0$), we have $\hat{\omega}_{*i} \bar{\omega}_{di} > 0$ and, since $\hat{\omega}_{*i} F_o \simeq -\bar{\omega}_{di} \partial F_{oi} / \partial \epsilon$, $\dfrac{\partial F_{oi}}{\partial \epsilon} \Big|_{\mu,L} < 0$. Equation (17), thus, indicates that resonant particles contribute to destabilization (stabilization) if $K\omega_r < 0 (> 0)$. For the $K\omega_r < 0$ destabilizing effect, the resonance condition, $\omega_r - \bar{\omega}_d - K\omega_b = 0$, becomes

$$\frac{\bar{\omega}_d}{\omega_r} = 1 - \frac{K\omega_b}{\omega_r} = 1 + \omega_b \left| \frac{K}{\omega_r} \right|. \qquad (18)$$

Equation (18) indicates that (i) only hot protons with $|\bar{\omega}_d / \omega_b|_{ih} \sim k_\perp \rho_{ih} \gtrsim |K|$ contribute to the destabilizing resonances, and (ii) $1 > \omega_r / \omega_{d,ih} > 0$, i.e., the excited instabilities have azimuthal phase velocities in the same direction but smaller than $v_{d,ih}$, which is westward propagating for energetic ring-current

protons. To understand the instability mechanism physically, let us assume $|\omega_r/\overline{\omega}_d| \ll 1$ and the resonance condition becomes $\overline{\omega}_d \simeq |K|\omega_b$. The resonant hot protons, thus, execute radial excursions in L while conserving $\mu$ and $\epsilon$ (instead of J). Noting that $\partial F_{oi}/\partial L|_{\mu,\epsilon} < 0$, the instability is, therefore, fed by the hot ion pressure gradient. Noting, furthermore, $\partial F_{oi}/\partial \epsilon < 0$ and the $J_o^2$ factor in Eq. (17), the $|k_\perp \rho_{ih}| \gtrsim |K|$ resonance constraint then implies that the $K = -1$ resonance term is the most important one. For a dipole **B** symmetric with respect to the geomagnetic equator at $\ell = 0$ (i.e., $\ell_1 = -\ell_T$ and $\ell_2 = \ell_T$), we can easily see from Eq. (17) that only odd $\widehat{\delta\phi}$ responds to the $K = -1$ resonance.

Assuming hydromagnetic waves with odd $\widehat{\delta\phi}$ are resonantly destabilized by the hot ions, let us now examine the stabilizing effects, which require $K\omega_r > 0$. The resonance condition then becomes $1 = \overline{\omega}_d/\omega_r + \omega_b|K/\omega_r|$ and $\overline{\omega}_d/\omega_r > 0$. Thus, only the warm ions contribute to the stabilization via the bounce resonances. Since in the presence ordering $|\omega/\omega_{b,iw}| \sim \delta^{1/2}$, the $K = 1$ term dominates.

To assess the relative importance of the hot-ion destabilization and warm-ion stabilization, we further assume $F_o$ for both warm and hot ions can be represented by a single Maxwellian distribution: $F_{oi} = n_{iw}(2\pi\epsilon_o)^{-3/2} \exp(-\epsilon/\epsilon_o)$, where $\epsilon_o(L)$ is the characteristic energy of ring-current protons. Assuming $k_\perp \simeq k_\phi$ with $\mathbf{e}_\phi = \mathbf{e}_L \times \mathbf{e}_\parallel$ in the westward direction and keeping only the $K = \pm 1$ terms, Eq. (17) becomes, approximately,

-12-

$$I_\beta \simeq I_{\beta i} \approx \beta_i \, |\delta\hat{\phi}|^2 \, (\frac{k_{\phi o}^2}{LB_o}) \{ J_o^2(1)(k_{\phi o}\rho_o)^{-7} \exp[-(k_{\phi o}\rho_o)^{-2}]$$

$$- (\frac{\omega_r}{\omega_{bo}})^7 \exp[-(\omega_r/\omega_{bo})^2] \} \, , \tag{19}$$

where $\rho_o = \sqrt{2\epsilon_o}/\Omega_{io}$, and $k_{\phi o}$ and $B_o$ correspond to equatorial values. Noting that, from Eq. (12), $\omega_r$ is independent of $k_\phi$, maximizing the destabilizing term in Eq. (19) then leads to

$$k_{\phi m}\rho_o \approx 0.5 \, . \tag{20}$$

We remark that, for ring-current protons at the geosynchronous orbit, we have typically $\epsilon_o \sim 30\,\mathrm{keV}$ and Eq. (20) then predicts $m \sim 0(10^2)$, which is consistent with satellite observations. With $k_{\phi o} \approx k_{\phi m}$, Eq. (19) shows that the instability threshold condition is essentially given by

$$|\frac{\omega_r}{\omega_{bo}}| < 1 \, . \tag{21}$$

Meanwhile, from Eq. (13), the growth rate is estimated to be

$$\omega_i \sim \beta_i (V_{Ao}/L)^2 / \omega_r \, . \tag{22}$$

Both Eq. (21) and Eq. (22) suggest that the most unstable mode is an odd-$\delta\hat{\phi}$ eigenmode with the lowest $\omega_r$. Now $\omega_r$ is given by Eq. (12) along with Eqs. (9) and (14). Since $|R_\beta| \sim 0(\beta) \sim 0(\delta) < 1$, the lowest-$\omega_r$ odd-$\delta\hat{\phi}$ mode tends to be the lowest antisymmetric mode, i.e., the second harmonic. However, $R_\beta$, can make significant corrections to $\omega_r$ and it is worthwhile to evaluate $R_\beta$ for the case of Maxwellian adiabatically injected particles and odd-$\delta\hat{\phi}$ eigenmodes.

First, we have from Eq. (9)

$$\delta\hat{\xi} = -\frac{1}{n_{oe}} <\omega_d F_o>_{ec} \delta\hat{\phi}.$$  (23)

Correspondingly, $R_\beta$ is then given by

$$R_\beta = (8\pi/c^2) \sum_{j=ew,iw} [(nq^2/m)| |\hat{\omega}_\kappa \omega_{*,t} |\delta\hat{\phi}|^2 | |]_j$$

$$+ [(4\pi q^2/mc^2\epsilon_o)| |(<\bar{\omega}_d - \omega_d)\omega_d F_o> |\delta\hat{\phi}|^2 | |]_{ic}$$

$$+ [(4\pi q^2/mc^2\epsilon_o)| |(<\bar{\omega}_d \omega_d F_o> - <\omega_d F_o>^2/n_o) |\delta\hat{\phi}|^2 | |]_{ec}.$$  (24)

Now, for a dipole magnetic field, one can readily show that $\omega_d(\ell)$ decreases away from the equator and, hence, $<(\bar{\omega}_d - \omega_d)\omega_d F_o>$ is positive (negative) away from (near) the equator. For an odd $\delta\hat{\phi}$, $|\delta\phi|^2$ is peaked away from the equator. We, therefore, expect $| |<(\bar{\omega}_d - \omega_d)\omega_d F_o> |\delta\hat{\phi}|^2 | | > 0$. Employing, furthermore, the inequality $<\omega_d^2 F_o> <F_o> \geq <\omega_d F_o>^2$ then demonstrates that all three terms in Eq. (24) are positive-definite, that is,

$$R_\beta > 0.$$  (25)

Thus, in the case considered here, both electrons and protons will contribute to a significant finite-$\beta$ reduction in $\omega_r$, which is destabilizing both in terms of reducing the bounce-resonance stabilization as well as enhancing the growth rate.

Finally, let us consider the compressional component, $\delta\hat{B}_{||}$, which from Eq. (10) is given by

$$\frac{\delta \hat{B}_{\parallel}}{B} = \frac{4\pi}{\omega B^2} \delta \hat{\phi} \{ [\frac{q_i}{\epsilon_0} < \frac{v_\perp^2}{2} \bar{\omega}_d F_0 > ]_{iw} + [\frac{q_i}{\epsilon_0} < \frac{v_\perp^2}{2} F_0 (\bar{\omega}_d - \omega_d) > ]_{ic}$$

$$+ q_e [\frac{1}{\epsilon_0} < \frac{v_\perp^2}{2} F_0 \bar{\omega}_d > - 2\omega_{\kappa,t} ]_e \}. \qquad (26)$$

Note that $\delta \hat{B}_{\parallel}$ is also antisymmetric as $\delta \hat{\phi}$. Both electrons and core ions, however, introduce additional structures along **B**. Neglecting these complexities, we have, approximately,

$$|\delta \hat{B}_{\parallel}| / |\delta \hat{B}_\perp| \approx 1.7 \beta, \qquad (27)$$

where we have assumed the ion pressure has $L^{-7.5}$ dependence and $k_{\parallel}L \sim 2$ for the second harmonic standing wave. Equation (27) indicates that the instabilities tend to have significant compressional components.

## SUMMARY AND DISCUSSIONS

In the preceding sections, we have presented a theory on the excitations of magnetospheric hydromagnetic waves by energetic ring-current particles. Since the theoretical approach employs the gyrokinetic equations, effects due to finite ion Larmor radii, realistic magnetic field geometries and plasma equilibria are included. By assuming a low-$\beta$ and isotropic plasma, the present work concentrates on excitations via wave-particle resonances. A reduced set of eigenmode equations is then derived by further assuming the plasma consists of core and energetic components. For adiabatically injected particles, the present theory predicts the following specific instability features: (1) destabilization via magnetic drift-bounce resonances of hot ions, $T_{ih} \sim O(10^2)$ keV; (2) the unstable eigenmodes are antisymmetric along **B** (i.e., odd $\delta \hat{\phi}$); (3) the most

-15-

unstable eigenmode tends to have $k_{\phi m}\rho_o \simeq 0.5$ and, correspondingly, the lowest real frequency; (4) the corresponding azimuthal phase velocity is in the same direction (i.e., westward) but smaller than the hot-ion magnetic drift velocity; (5) the instability, in general, has significant transverse and compressional components; and, finally (6) finite-$\beta$ (plasma pressure) values can significantly reduce the real frequencies. These features, we note, are consistent with satellite observations mentioned earlier.

The apparent success of the present theory has obviously motivated us to examine the more general case of a $\beta \sim 0(1)$, anisotropic plasma, where one, perhaps, can hope for a description unifying destabilizing mechanisms due to both velocity-space anisotropy (i.e., the drift mirror mode) and wave-particle resonances. This attempt for a unified description is currently in progress and the results will be presented in a future publication.

## ACKNOWLEDGEMENTS

-16-

# REFERENCES

Allan, W., E. M. Pulter, and E. Nielsen, STARE Observations of a Pc5 pulsations with large anzimuthal wave number. *J. Geophys. Res.* *87*, 6163 (1982).

Antonsen, T. M., Jr., and B. Lane, Kinetic equations for low frequency instabilities in inhomogeneous plasmas, *Phys. Fluids 23*, 1205 (1980); Catto, P. J., W. M. Tang, and D. E. Baldwin, Generalized gyrokinetics, *Plasma Phys. 23*, 639 (1981).

Hasegawa, A., Drift mirror instability in the magnetosphere, *Phys. Fluids 12*, 2642 (1969).

Meerson, B. I., A. B. Mikhailovskii, and O. A. Pokhotelov, Excitation of Alfven waves by fast particles in a finite pressure plasma of adiabatic traps, *J. Plasma Phys. 2*, 137 (1978).

Southwood, D. J., A general approach to low frequency instability in the ring current plasma, *J. Geophys. Res. 81*, 3340 (1976).

Takahashi, K., P. R. Higbie, and D. N. Baker, Azimuthal Propagation and frequency characteristics of compressional Pc5 waves observed at geostationary orbit, *J. Geophys. Res. 90*, 1473 (1985).

Takahashi, K., and P. K. Higbie, Antisymmetric standing wave structure associated with the compressional Pc5 pulsation of November 14, 1979, *J.*

*Geophys. Res. 91*, 11163 (1986); Takahashi, K., J. F. Fennell, E. Amata. and P. R. Higbie, Field-aligned structure of the storm time Pc5 wave of November 14-15, 1979, *J. Geophys. Res. 92*, 5857 (1987).

Walker, A. D. M., R. A. Greenwald, A. Korth, and G. Kremser. STARE and GEOS 2 observations of a storm time Pc5 ULF pulsations., *J. Geophys. Res. 87*, 9135 (1982); Pokhotelov, O. A., V. A. Pilipenko. Yu. M. Nezlina. J. Woch, G. Kremser, and A. Korth, Excitation of high-$\beta$ plasma instabilities at the geostationary orbit: theory and observations. *Planet. Space Sci. 34*, 695 (1986).

# SECTION II: PLASMA-WALL PHYSICS, THEORY AND SIMULATION

## A.    Multi-Scale Particle Simulation of Bounded Plasmas

*S. E. Parker and C. K. Birdall, UC-Berkeley,*
*A. Friedman and S. L. Ray, LLNL*

Our basic goal is to study the kinetic behavior of a bounded plasma. including

the boundary layer (or sheath) effects. We want to understand how the bulk plasma

behavior with long space and time scales interacts with the boundary layer where

short space scales ($\sim \lambda_{De}$), and time scales ($\sim \omega_{pe}^{-1}$) are important. Currently.

explicit codes have been successful at modeling the sheath dynamics for system

lengths less than 100 $\lambda_{De}$[1]. These codes have a constraint on $\omega_{pe}\Delta t$ for stability

and accuracy which restricts them to short systems and times  The newer Direct

Implicit Codes[2,3] have been successful at relaxing the $\omega_{pe}\Delta t$ constraint for stability.

but are restricted by accuracy to small $kv_{Te}\Delta t$. where $k^{-1}$ is the characteristic scale

length of the electric field. Typically. $k^{-1}$ would be the order of $\lambda_{De}$ in the sheath

region, hence, rewriting $kv_{Te}\Delta t = (k\lambda_{De})(\omega_{pe}\Delta t)$. we see that short time steps are

necessary to resolve the sheath. Thus. if one needs to model the boundary layer

accurately, the implicit method has no advantage.

The constraint on a individual particle with velocity $v$ is $kv\Delta t$. This assures

proper sampling of the electric field. Since the most severe restriction on $kv\Delta t$ is local to the boundary, we can take advantage of this and move particles at different time scales depending on their location in phase space (x,v). We term this the *Multi-Scale Method*[4]. The majority of the electrons are in the bulk plasma region where nonuniformity in field and density are mild compared to the sheath region. All of the ions and most of the electrons can be moved much less frequently than the minority of fast time scale electrons. By allowing the time step at which particles are moved to vary, we can greatly reduce computing time and permit modeling of larger systems.

Our model is one dimensional, electrostatic, unmagnetized, and collisionless (We intend to include Coulomb collisions in the future). The boundaries are absorbing and there is a prescribed distributed source, $S(x,v;t)$. One motivating application is the flow of a plasma along magnetic field lines to a conducting wall. This problem is important for the understanding of how plasma flows to the divertor plate or limiter in a Tokamak fusion device[5]. One is interested in how the boundary layer effects the bulk plasma.

**Current Progress**

We have developed a bounded one dimensional electrostatic particle simulation that uses the Direct Implicit Method[6]. A consitant way of prescribing the boundary conditions when using the Direct Implicit Method has been developed. Test runs

show that the sheath is not properly resolved which motivates implementation of the Multi-Scale Method.

A periodic code called MIST (Multi-Scale Implicit Testbed) is being developed to test the Multi-Scale Technique*. The algorithm has been worked out and is explained in Reference 4. One of the current research issues is the criterion for choosing a particles $\Delta t$, see Reference 7.

## References

[1] "Collector and Source Sheaths of a Finite Ion Temperature Plasma Including Secondary Electron Emission and Ion Reflection at the Collector Surface". L. A. Schwager, Ph. D. Dissertation, October. 1987.

[2] "Direct Implicit Particle Simulation", A.B. Langdon, D.C. Barnes. from *Multiple time scales*. J.U. Brackhill and B.I. Cohen. editors. Academic Press. 1985.

[3] "Direct Implicit Large Time-Step Particle Simulation of Plasmas". A.B. Langdon, B.I. Cohen. and A. Friedman, JCP **51** 107-138 (1983).

[4] "Prospects for Multi-Scale Particle-in-Cell Simulation of Plasmas". A. Friedman. S.L. Ray. S.E. Parker. and C.K. Birdsall. APS-DPP poster session. November 1987.

[5] "Plasma Flow in the Sheath and Presheath of a Scrape-off Layer", R. Chodura. from *Physics of Plasma-Wall Interactions in Controlled Fusion*. D. E. Post and R. Behrisch. editors. Plenum Press, 1984.

[6] "Direct Implicit Particle Simulation of a Bounded Plasma System". S. E. Parker. C. K. Birdsall. A. Friedman. and S.L. Ray. APS-DPP poster session. November 1987.

[7] "Multi-Scale Particle-In-Cell Plasma Simulation: Timestep Control Criteria and Some Tests", A. Friedman. S.L. Ray, C. K. Birdsall. and S. E. Parker. IEEE Plasma Science Conference, June 1988.

## B.  Numerical Error in Electron Orbits with Large $\omega_{ce}\Delta t$

*S. E. Parker and C. K. Birdsall*
*Electronics Research Laboratoy, U.C. Berkeley*
*Berkeley, California 94720*

**Introduction**

We have been using a bounded 2d electrostatic particle simulation[1] to study electrostatic effects induced by nonuniform magnetic fields[2]. It was found that running with large values of $\omega_{ce}\Delta t$ did not seem to pose any significant problems in our model. The work presented here is to address why plasma simulation with large $\omega_{ce}\Delta t$ under controlled circumstances can give good results.

When simulating a magnetized plasma with electron inertial effects included. the limiting time scale in many situations is the electron cyclotron period. with a constraint on $\omega_{ce}\Delta t$. If one is not interested in short time scales. this restraint can make simulation of other effects at longer time scales. e.g. ion transit times. very expensive. Particle simulation has been done using the guiding center equations for electrons[3] to relax the $\omega_{ce}\Delta t$ constraint. Alternately. we are exploring the feasibility of running with large $\omega_{ce}\Delta t$ using the standard integration scheme of Boris[4]. We begin by comparing single particle orbits with large $\omega_{ce}\Delta t$ to those with small $\omega_{ce}\Delta t$. Then. the error introduced when $\omega_{ce}\Delta t$ is large is discussed.

**Results from a single particle mover for $\omega_{ce}\Delta t \gg 1$**

To study the errors introduced with large $\omega_{ce}\Delta t$, we used a single particle mover with two spatial coordinates, $(x, y)$ and, three velocity coordinates, $(v_x, v_y, v_z)$. The following parameters are the same in all the runs: $\mathbf{v}(t = 0) = (0.1, 0.0, 0.4)$ and. $\frac{e}{m} = 1$. The magnetic field, electric field, and time step is varied. Figure 1 has two runs with $\omega_{ce}\Delta t = 0.5$ and 50; $\mathbf{B} = (250, 0, 0)$, and $\mathbf{E} = (0, 0, 1)$ for both runs. $\mathbf{v}_{DE} = 0.004\hat{y}$ as predicted. For the run with $\omega_{ce}\Delta t = 50$; $r_{g,eff} \approx v_\perp \Delta t$. and $w_{c,eff} \approx 0.04$ as expected from the discussion below. Figure 2 has two runs with $\omega_{ce}\Delta t \approx 0.5$ and 50. In these runs the magnetic field is nonuniform and there is no electric field. Note that the averaged orbits are approximately equal.

**Single particle orbits with $\omega_{ce}\Delta t \gg 1$**

In this section we characterize the electron orbit when $\omega_{ce}\Delta t$ is large. The $\mathbf{v} \times \mathbf{B}$ integration scheme gives the angle of rotation for one time step as[4]:

$$\theta = 2\arctan\left(\frac{1}{2}\omega_{ce}\Delta t\right) \qquad (1)$$

As $\omega_{ce}\Delta t \to \infty$, $\theta \to \pi$. The orbit for $\omega_{ce}\Delta t \gg 1$ can be described as rapid bounce back and forth motion with the perpendicular velocity. and a slow precession about the guiding center axis. For large $\omega_{ce}\Delta t$, the angle of rotation is approximately:

$$\theta \approx \pi - \frac{4}{\omega_{ce}\Delta t} \qquad (2)$$

The precession is the result of the rotation angle being a small amount $\delta$ less than $\pi$, $\delta \approx \pi - \theta$. The frequency of this precession is:

$$\omega_{prec} = \frac{\delta}{\Delta t} \approx \frac{4}{\omega_{ce} \Delta t} \tag{3}$$

The "effective" cyclotron frequency is just $\frac{\theta}{\Delta t}$, or:

$$\omega_{c,eff} \approx \frac{1}{\Delta t}\left(\pi - \frac{4}{\omega_{ce}\Delta t}\right) \tag{4}$$

for large $\omega_{ce}\Delta t$. The "effective" gyroradius for all values of $\omega_{ce}\Delta t$ is given by:

$$r_{g,eff} = \frac{v_\perp \Delta t}{2\sin\left(\frac{1}{2}\theta\right)} = r_{g,eff}\left[1 + \left(\frac{\omega_{ce}\Delta t}{2}\right)^2\right]^{\frac{1}{2}} \tag{5}$$

Hence $r_{g,eff} \sim O(\Delta t)$, and can be made small if it is a major cause of noise in the simulation model. Note that $w_{c,eff}$ goes to $\frac{\pi}{\Delta t}$ for large $\omega_{ce}\Delta t$.

## Guiding center motion with $\omega_{ce}\Delta t \gg 1$

Let us analyze the guiding center motion to see what error is introduced when $\omega_{ce}\Delta t$ is made large. We start with the integration scheme eliminating $\mathbf{v}$ using $\mathbf{v}^{n-\frac{1}{2}} = (\mathbf{x}^n - \mathbf{x}^{n-1})/\Delta t$ and, $\mathbf{v}^{n+\frac{1}{2}} = (\mathbf{x}^{n+1} - \mathbf{x}^n)/\Delta t$:

$$\frac{1}{\Delta t^2}\left(\mathbf{x}^{n+1} - 2\mathbf{x}^n + \mathbf{x}^{n-1}\right) = \frac{q}{m}\left\{\mathbf{E}(\mathbf{x}^n) + \frac{1}{2\Delta t}(\mathbf{x}^{n+1} - \mathbf{x}^{n-1}) \times \mathbf{B}(\mathbf{x}^n)\right\} \tag{6}$$

Let the magnetic field $\mathbf{B}$ be in the $x - y$ plane and define the following coordinates: $\hat{\mathbf{e}}_1 = \frac{\mathbf{B}}{B}$, $\hat{\mathbf{e}}_2 = \hat{z}$, and $\hat{\mathbf{e}}_3 = \hat{\mathbf{e}}_1 \times \hat{\mathbf{e}}_2$. Let $\mathbf{x}^n = \mathbf{x}_0^n + \mathbf{x}_1^n$, where $\mathbf{x}_1^n = r_{g,eff}(sin\phi\hat{\mathbf{e}}_2 + cos\phi\hat{\mathbf{e}}_3)$, and $\phi = \phi_0 + \Delta t \sum \omega_{c,eff}(t^n)$. $\mathbf{x}_0$ is the slowly varying guiding center

motion, and $\mathbf{x}_1$ is the fast gyration. Assume that $\omega_{c,eff}$ does not vary much between time steps so we can use the approximation $\omega_{c,eff}(t^n) \approx \omega_{c,eff}(t^{n+1})$. Taking a Taylor series expansion of equation (5) about $\mathbf{x}_0$, and then equating the slowly varying terms gives the guiding center equation:

$$\frac{1}{\Delta t^2}\left(\mathbf{x}_0^{n+1} - 2\mathbf{x}_0^n + \mathbf{x}_0^{n-1}\right) = \frac{q}{m}\left\{\mathbf{E}(\mathbf{x}_0^n) + \frac{1}{2\Delta t}(\mathbf{x}_0^{n+1} - \mathbf{x}_0^{n-1}) \times \mathbf{B}(\mathbf{x}_0^n)\right\} - \frac{\mu_{eff}}{m}\nabla B(\mathbf{x}_0^n)$$

$$+ O\left(\frac{q}{m}r_{g,eff}^2\right) \tag{7}$$

where $\mu_{eff} = \frac{qr_{g,eff}^2}{2\Delta t}sin(\omega_{c,eff}\Delta t)$. Using equations (3) and (5), we get $\mu_{eff} = \frac{1}{2}\frac{v_\perp^2}{B} = \mu$. The guiding center equation of motion given by Northrup[5] is:

$$\frac{d^2\mathbf{x}_0}{dt^2} = \frac{q}{m}\left\{\mathbf{E}(\mathbf{x}_0) + \frac{d\mathbf{x}_0}{dt} \times \mathbf{B}(\mathbf{x}_0)\right\} - \frac{\mu}{m}\nabla B(\mathbf{x}_0) + O\left(\frac{q}{m}r_g^2\right) \tag{8}$$

Equation (7) is just a central difference approximation to equation (8). Hence, we expect the same first order drift motion.

**Conclusions and future work**

We conclude that even with $\omega_{ce}\Delta t \gg 1$ the Boris algorithm still gives the correct guiding center motion for a single particle. This paper did not take into account the collective error introduced by a large number of particles. We need to examine collective numerical instability.

A possible improvement that would eliminate the $\omega_{ce,eff}$ and $r_{g,eff}$ effects on the fields would be to subtract off the rapid bounce motion before the wieghting of

particles to calculate the charge density.

$$x_f^n = x^n - \frac{1}{2}v_\perp^{n-\frac{1}{2}}\Delta t \tag{9}$$

Where the $f$ subscript represents the position for particle wieghting for the charge density. It would only apply when $\omega_{ce}\Delta t \gg 1$. This is just a suggestion and needs to be tested as part of our future work.

## References

[1]    "ES2 User's Manual - Version 1", K. Theilhaber, E.R.L. Report, U.C. Berkeley, May 1987.

[2]    "Electrostatic confinement due to nonuniform magnetic fields with application to FRC confinement", S. Parker, K. Theilhaber, and C. K. Birdsall. Poster session, APS-DPP conference, November 1986.

[3]    "A simulation model for studying low frequency microinstabilities", W. W. Lee and H. Okuda. JCP **26**, 139 (1978).

[4]    *Plasma physics via computer simulation*, C. K. Birdsall and A. B. Langdon, p.58-62, McGraw-Hill, New York, 1985.

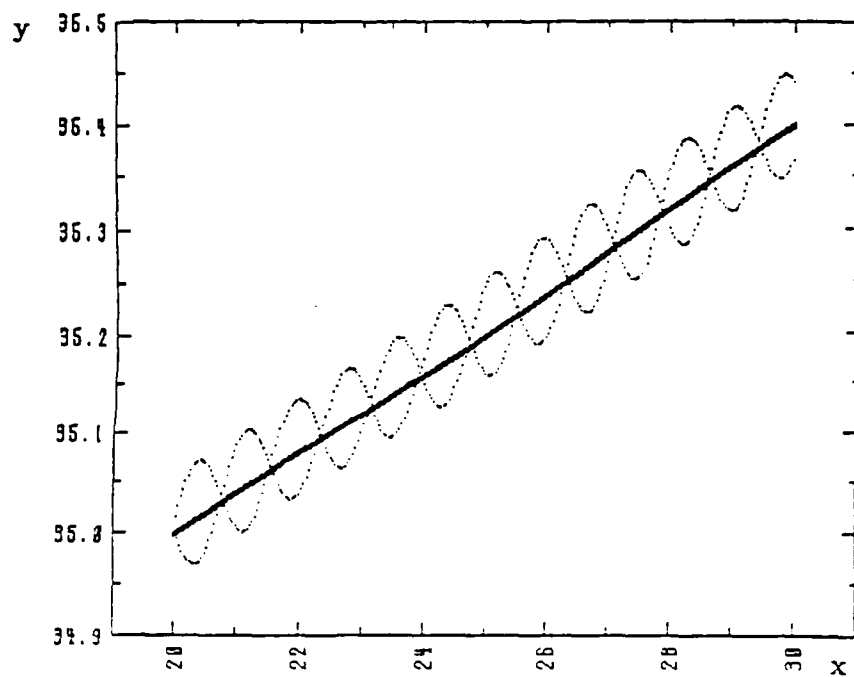[5]    *The adiabatic motion of charged particles*, T. H. Northrop, J. Wiley and Sons, New York, 1963.

Figure 1. E×B drift with $\omega_{ce}\Delta t = 0.5$ and 50.



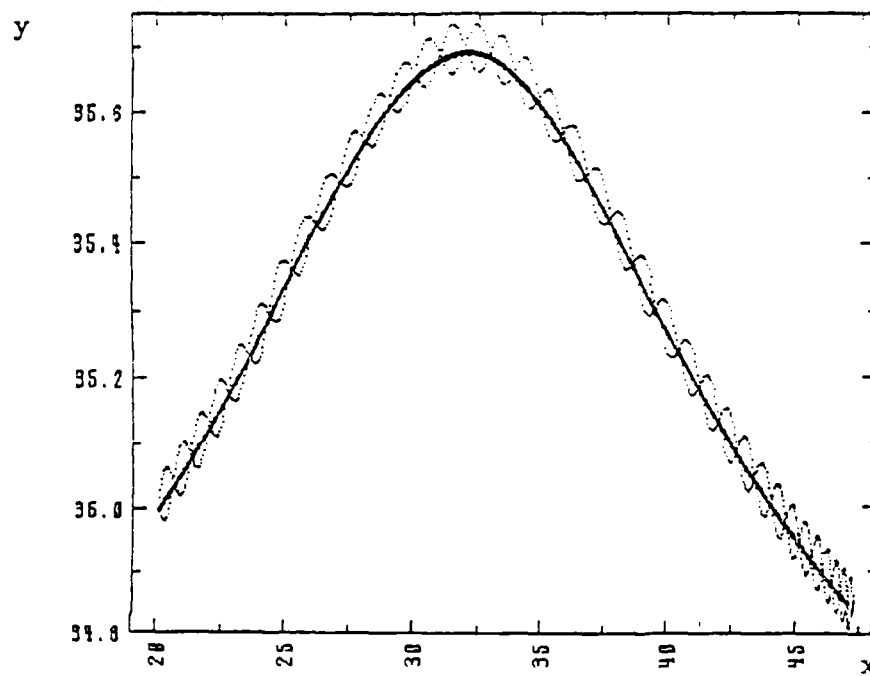Figure 2. Nonuniform Magnetic field with $\omega_{ce}\Delta t \approx 0.5$ and 50.

## C. Electron-Neutral Particle Collisions in ES1

*Julia Little*

### 1. Introduction

We are adapting ES1 to incorporate electron-neutral particle collisions. In the formulation of the problem, we assert that the collisions are elastic since the mass of the electron is negligible when compared to the mass of the neutral particle. We note that the radiation process, considered to be negligible, is omitted[1]. We also note that electron-molecule collisions are more complicated than electron-atom collisions[1], but we treat only the electron-atom collisions.

The electron-neutral collisions are modelled with electrons scattering off a fixed background of neutrals as if the neutrals are hard and massive spheres. Scattering angles are chosen uniformly randomly in the interval 0 to $\pi$ and phase angles are chosen uniformly randomly in the interval 0 to $2\pi$. The details of the simulation of hard sphere scattering and of the method of deciding when an electron will scatter are described in the next two sections. In the fourth section, we discuss how the computer routine modelling electron-neutral collisions in the above manner was tested and showed some expected statistics for the angular spread in time of a beam of virtually ballistic particles. Finally, we will suggest further improvements and uses of ES1 with the elastic collisions.

The model above does not handle charge exchange between species or ionization and excitation of neutrals. However, we believe it is a good first step for the effect of elastic

-28-

collisions on the plasma behavior in the regime where electron-neutral collisions exceed Coulomb collisions, as is true for weakly ionized plasmas.

## 2. The Model and Simulation of Hard Sphere Scattering

We essentially use the scattering routine written in 1985 by Perry Gray for use in PDW1 but with minor changes. Since ES1 is a one dimensional program, only the $x$ component of velocity, $v_x$ is used in finding the new position for a particle. (If the plasma is magnitized. then the $y$ component of the velocity, $v_y$ is needed for the $\mathbf{v} \times \mathbf{B}$ force. but again only $v_x$ is used to advance the particle's position.)

In our program, however, when an electron is to collide with a neutral. we include $v_y$ and introduce a $z$ component of velocity, $v_z$. (See Fig.1) (Initially, we set $v_y$ to 0 for all particles if the plasma is unmagnitized. Otherwise. the determination of the initial values of $v_y$ is left unchanged. We give $v_z$ a Maxwellian distribution if the plasma is warm and otherwise set $v_z$ to 0.) Prior to making a collision. ES1 assumes the velocity vector. $v$ has components on a sphere of radius $|v|$, where $|v|$ is the magnitude of $v$:

$$v_x = |v|\cos\alpha,$$

$$v_y = |v|\sin\alpha\cos\beta, \text{ and}$$

$$v_z = |v|\sin\alpha\sin\beta.$$

Then the scattering angle, $\gamma$ and the phase angle, $\delta$ are both chosen uniformly randomly in the interval 0 to $\pi$ and 0 to $2\pi$, respectively. Hence after the collision the new values for the velocity components become

$$v_{x_{coll}} = |v|\cos\gamma,$$

$v_{y_{coll}} = |v|\sin\gamma\cos\delta$, and

$v_{z_{coll}} = |v|\sin\gamma\sin\delta$.

Note that the magnitude of the velocity of a particle remains constant for all time steps. Hence, the effect of an electron-neutral collision is the rotation of $v$ through a uniformly random angle about a sphere of radius $|v|$. Only the direction of $v$ changes and not its magnitude.

### 3. How The Decision Of Which Electron Is To Collide Is Made

Given a physical system of electrons and neutrals including electron-neutral collisions, an upper estimate of the collision frequency, $\nu$ must be made in advance in order to appropriately determine the time step, $\Delta t$ to be used in the simulation. For example, one may want approximately all particles to collide in 100 time steps. Given $\nu$ by the physics of the system, then $\Delta t$ is determined from the equation $\nu\Delta t = \frac{1}{100}$. (Actually, one approximates the relative velocity of the electron with the neutral, $v_{rel}$ and the mean free path for the system, $\lambda_{mfp}$ and solves $\frac{v_{rel}}{\lambda_{mfp}}\Delta t = \frac{1}{100}$ for $\Delta t$, since $\nu = \frac{v_{rel}}{\lambda_{mfp}}$. Consequently, a convenient input parameter for ES1 with elastic collisions is the inverse of the mean free path, $\frac{1}{\lambda_{mfp}}$.)

Having chosen $\Delta t$, we are now able to assign a probability of collision to an electron in such a way that the probability of the electron colliding is a function of its velocity. If the magnitude of its velocity vector, $|v|$ is large, the probability of collision will be high and if the magnitude is small, the probability of collision will be low. That is, for each particle and at each time step we choose a uniformly random number, $r$ and if $r \leq \frac{1}{\lambda_{mfp}}|v|\Delta t$, the

particie will collide according to the scattering procedure described in the previous section. Otherwise, the particle will not collide and no adjustments will be made to $v_x, v_y$, and $v_z$.

## 4. Testing The Collision Model On a Beam Of Electrons

To test ES1 with electron-neutral colisions, we made 4 runs, each of which started out with a mono-energetic beam of electrons (at time zero $v_x = 1$, $v_y = 0$ and $v_z = 0$). In all runs the plasma frequency, $\omega_p$ was set to $10^{-12}$ so that the measure of any fields would be negligible. The effect was to make the electrons virtually chargeless and hence to make the electron-neutral collisions ballistic. Also, for all runs the length of the system, $l$ was 1. The four runs differed by the following parameters:

$$1. \nu \Delta t = \tfrac{1}{100}, \tfrac{l}{\lambda_{m/p}} = 5$$

$$2. \nu \Delta t = \tfrac{1}{100}, \tfrac{l}{\lambda_{m/p}} = 1$$

$$3. \nu \Delta t = \tfrac{1}{10}, \tfrac{l}{\lambda_{m/p}} = 5$$

$$4. \nu \Delta t = \tfrac{1}{10}, \tfrac{l}{\lambda_{m/p}} = 1$$

In all four cases we measured the increase of the distribution function of $v_x$, $f(v_x)$ at $v_x = -1.0$ and the decrease of $f(v_x)$ at $v_x = 1.0$ verses time. (See Figs. 2a through 2d) We found that both sets of measurements seemed to approach asymptotically the same value with increase in time, as expected. Then we measured the growth rates of $f(v_x = -1.0)$ for the first few time steps and found that they agreed well with theory.

## 5. Conclusions

We feel confident that the scattering routine works effectively in ES1. The routine remains to be tested on a plasma with fields and also for large $\nu \Delta t$ or where $l \ll \lambda_{mfp}$.

Also, the procedure for deciding whether or not an electron with a given velocity collides eventually can be made vectorizable.

## 5. Acknowledgments

**References**

[1] *The Particle Kinetics of Plasmas*, Shkarofsky, Johnston and Bachynski. Chap. 5. Addison-Wesley Publishing Co., Inc., 1966.

[2] "Elastic Collisions in Simulating One-imensional Plasma Diodes on the Computer". P. Burger. Phys. Fl. 10 pp. 658-665. March 1967.

[3] "EECS 290Q Notes". C. K. Birdsall and A. B. Langdon. Section 4.14 (by W. Nevins and J. Harte).

[4] "One Dimensional Model of a Lorentz Plasma". R. Shanny. J. M. Dawson. J. M. Greene. Phys. Fl. 10 pp. 1281-1286. June 1967.
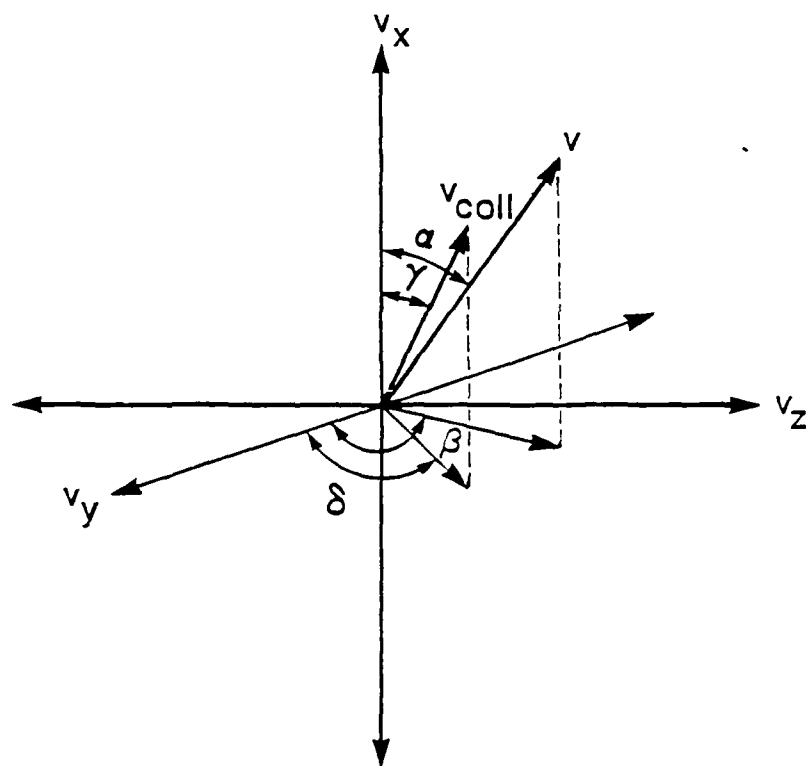
Figure 1. Velocity angles for electron-neutral elastic scattering. The initial velocity
is $v$ and the final velocity is $v_{coll}$, same magnitude by different angle.
The scattering is "large angle," not "cumulative small angle", as with
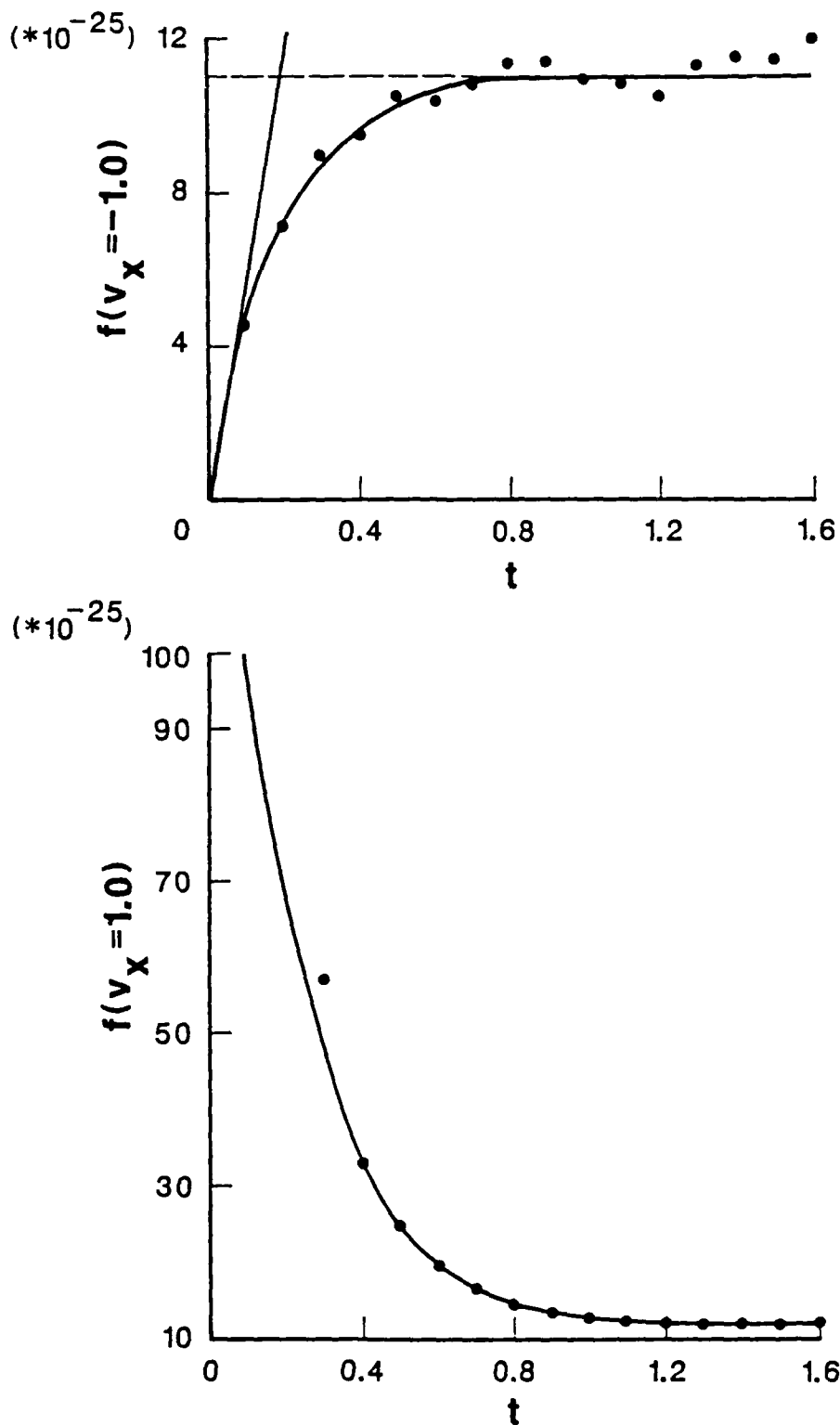Coulomb collisions.

Figure 2a.  Values of $f(v_x)$ for all particles initially at $v_x=1.0$, at $v_x=1.0$ and $v_x=-1.0$.  The latter rises proportional to $(1-e^{-vt})$; for small $vt$ this is just $vt$ so that the crossing of this line and unity occurs at $t=1/v$.  Here the crossing is at $t=0.2$, so $v=5$, which is just $v_{rel}/\lambda_{mfp}$, a direct confirmation.  After $t=0.8$, particles are uniformly spread over the sphere $v=1$.
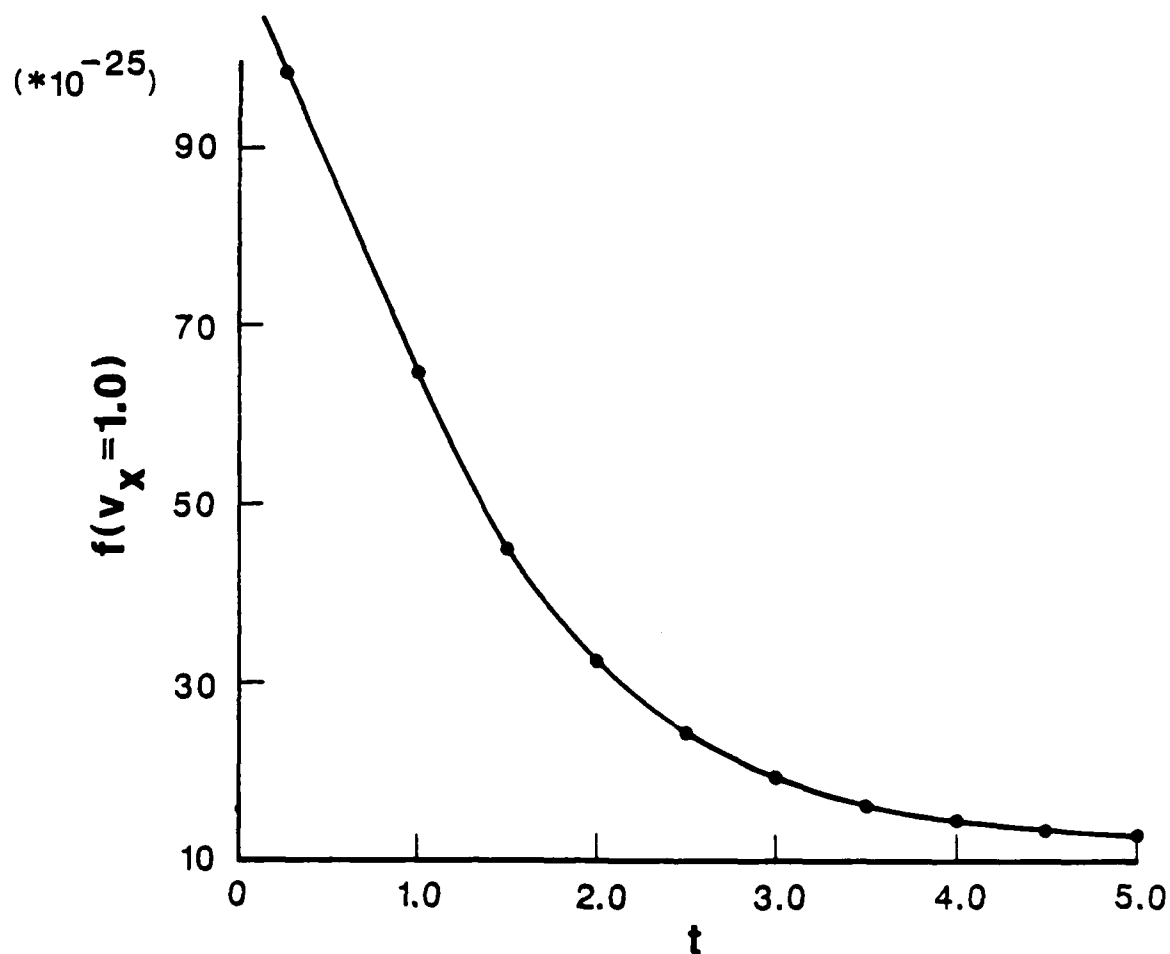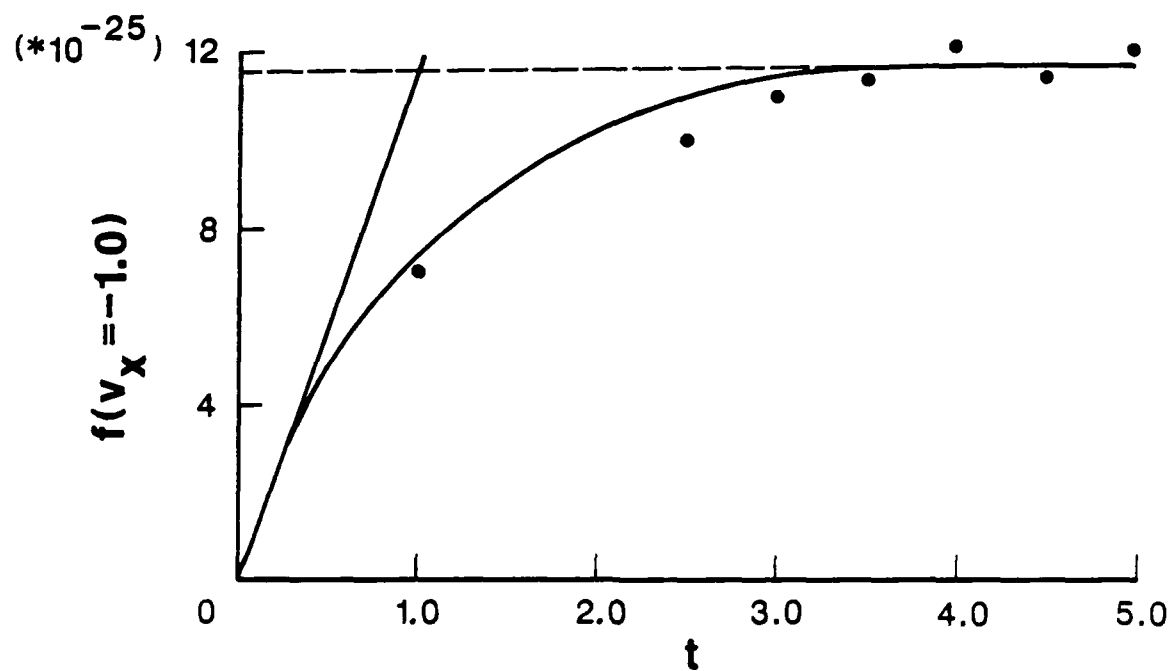
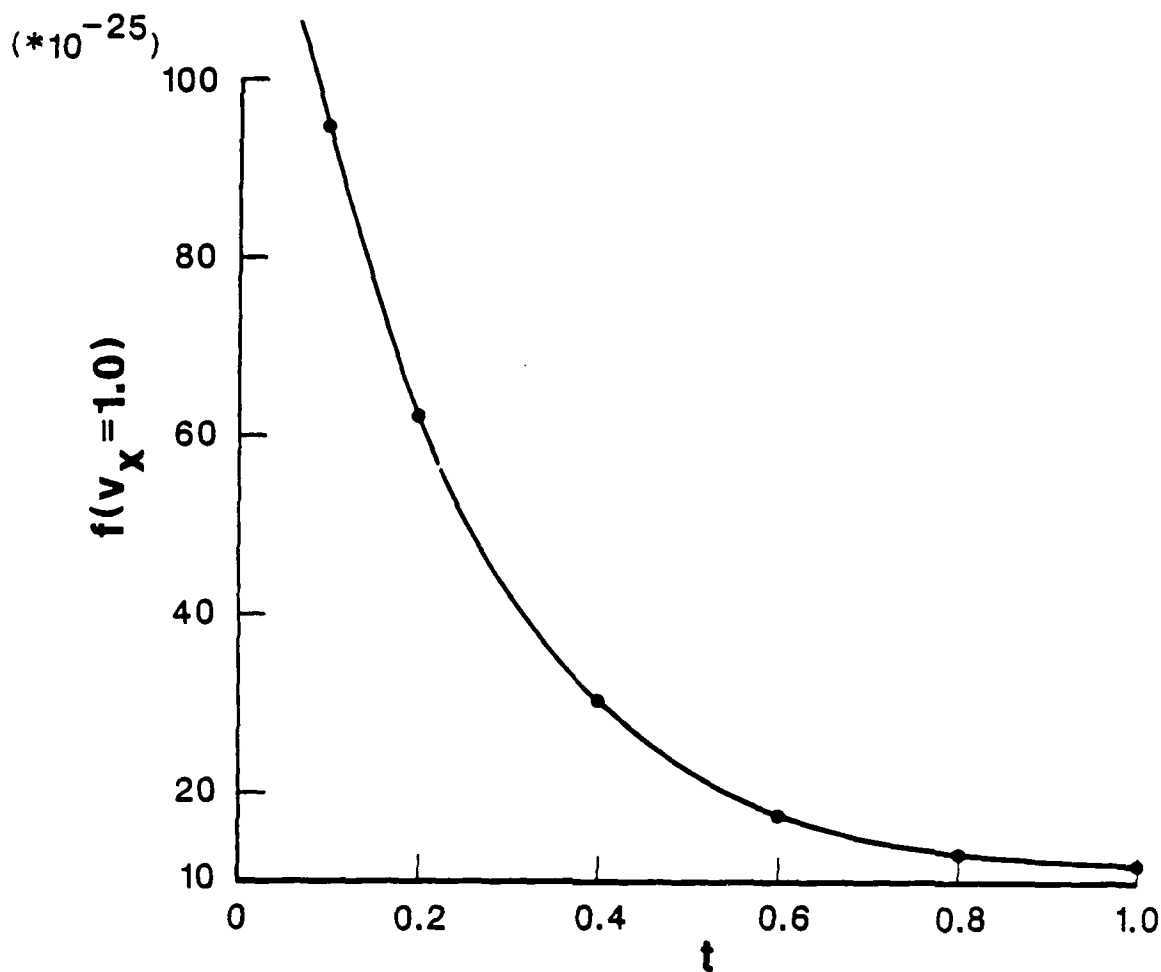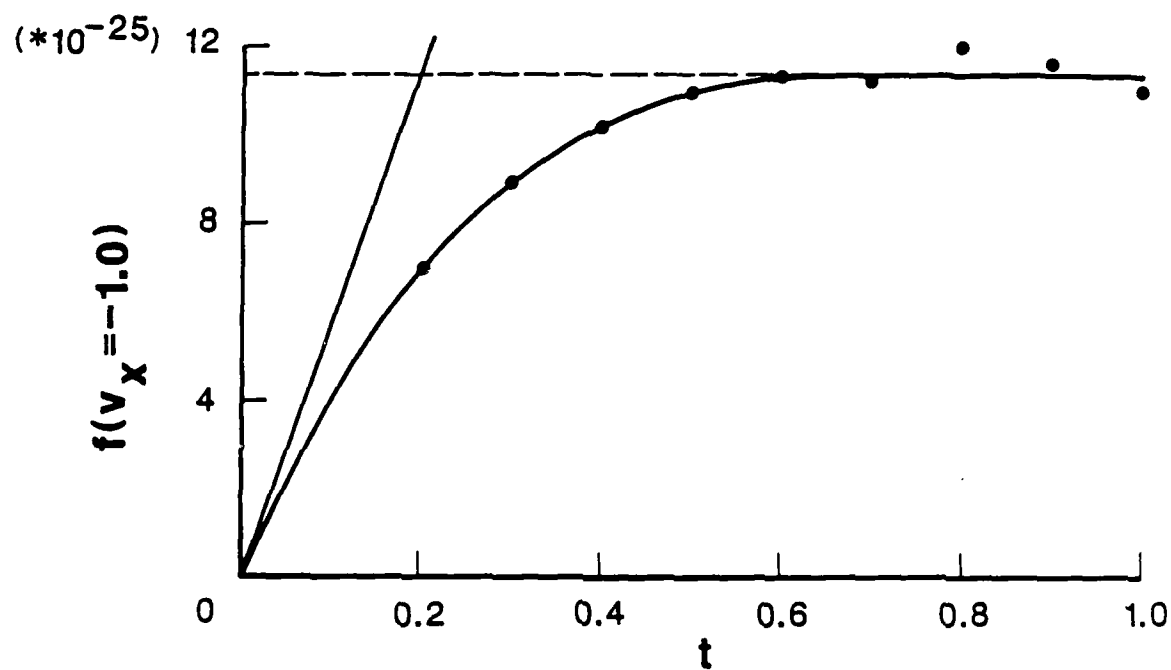Figure 2b.  Here with $v/\lambda_{mfp}$ is 1.0 and indeed $v=1$ is observed.

Figure 2c.    Here $\nu/\lambda_{mfp}$ is 5 and again $\nu=5$ is observed.
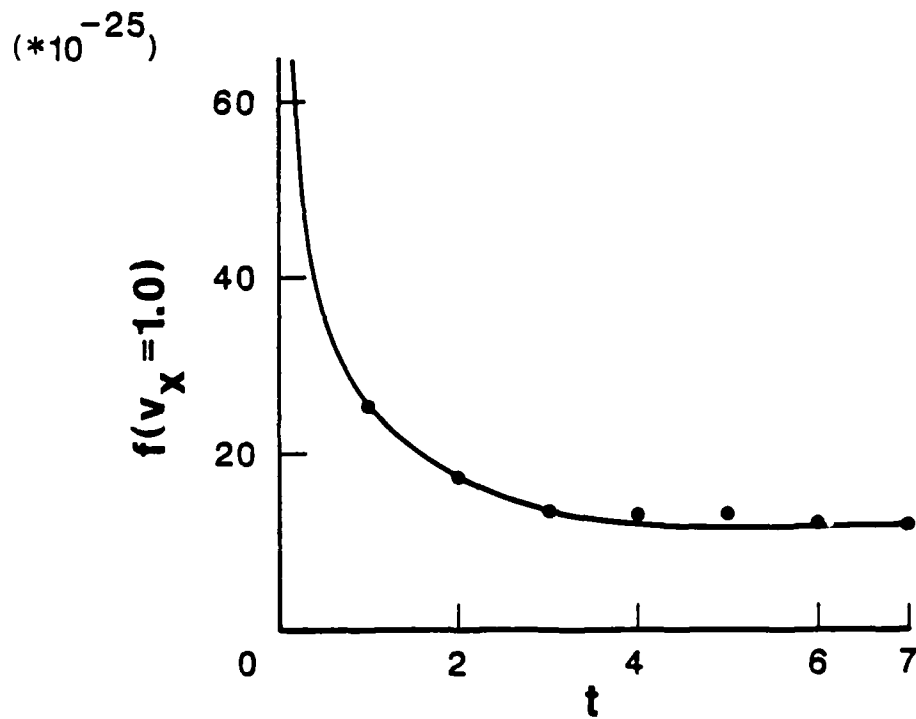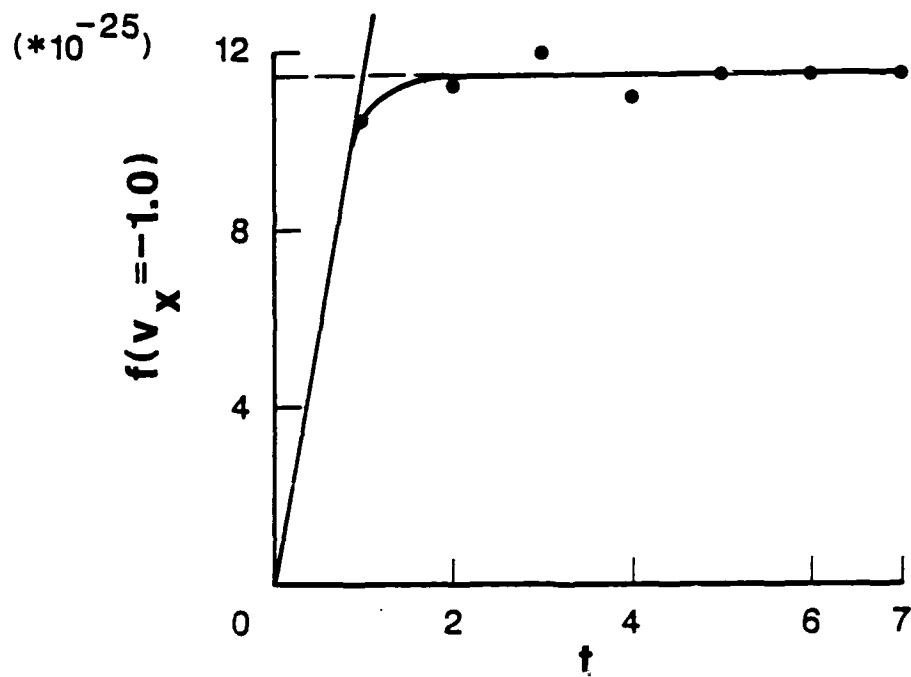
Figure 2d.   Here $v/\lambda_{mfp}$ is 1.0 and $v=1$ is observed.

# D. Particle-In-Cell Simulations of Radiofrequency Heating (ECRH) of a Simple Mirror Plasma

*R. J. Procassini, J. C. Cummings*

*and*

*B. I. Cohen (Lawrence Livermore National Laboratory)*

## Introduction

Particle confinement in mirror plasmas is based upon the conservation of kinetic energy and the adiabaticity of the magnetic moment, such that the particles bounce back and forth in the magnetic potential well. Only a certain fraction of the particles are trapped or confined by this potential well. The trapped region in $v_\perp$ vs. $v_\parallel$ space is defined by the mirror magnetic field ratio and the plasma ambipolar electrostatic potential. The main loss mechanism for particles in both simple mirror plasmas and in the end plugs of tandem mirror plasmas is collisional detrapping of the particles from this trapped region into the loss cone. Once in the loss cone, the particles are free to transit out the ends of the device, unhindered by the magnetic field.

Ions in the center cell region of a tandem mirror device are electrostatically confined by large positive ambipolar potentials which arise in the end plugs of the device. In the simplest model, this potential increases linearly with the electron temperature in the end plugs.

It is possible to improve particle confinement in mirror devices through the injection of radiofrequency waves at the fundamental or some harmonic of the electron cyclotron freqeuency. This process is termed Electron Cyclotron Resonance Heating (ECRH). The increase in the confinement of center cell ions in a tandem mirror is due to the heating of the plug electrons, which results in an increase in the confining electrostatic potential in the plugs. Of secondary interest is the enhancement of electron confinement in a simple mirror or tandem mirror plug, which is due to the preferential increase of the perpendicular velocity relative to the parallel velocity. This leads to hot electrons which are placed farther into the trapped region of velocity space, thereby requiring a longer time to collisionally migrate to the loss boundary in velocity space. This assumes that the hot electrons remain microstable.

## Methodology

The TESS (Tandem Experiment Simulation Studies) code is being developed to investigate thermal-barrier formation and particle confinement in a tandem mirror plasma. TESS is a 1D-3V (one spatial dimension, three velocity component) guiding-center, relativistic, electrostatic particle code, which includes a Monte Carlo binary particle collision package, a neutral-beam heating package and a radiofrequency (RF) heating package, which is the focus of this paper.

The RF-heating package is based upon the quasilinear model of Berstein and

Baxter[1], which treats the heating of mirror-trapped particles. The model is valid for mildly relativistic electrons in the presence of a cyclotron resonant applied electromagnetic field. The model assumes that the cyclotron frequency is much higher than the bounce frequency in the magnetic potential well, and then averages over the particle trajectories as they bounce in the well. One of the main results of Reference 1 is the derivation of a quasilinear diffusion equation which describes the slow evolution of the heated electron distribution function $f_o$ in $\epsilon$ (total energy) . $\mu$ (magnetic moment) space.

The RF-heating model was incorporated into the particle code in the following way. The region over which the RF power is being injected is defined by a center location $Z_{o_{RF}}$ and a width $\Delta Z_{RF}$. The intensity of the injected RF power varies within the region as

$$E_{RF}(z) = \frac{E_{RF}(Z_{o_{RF}})}{2} \left[ 1 + cos\left( \frac{2\pi(z - Z_{o_{RF}})}{\Delta Z_{RF}} \right) \right] \qquad (1)$$

where $E_{RF}(Z_{o_{RF}})$ is the maximum amplitude of the RF wave within the region. Particles which lie within this region are tested to determine if they meet the resonance condition $\mathbf{R} = 0$, where

$$\mathbf{R} = \omega_{RF} - \frac{\ell\Omega_s}{\gamma} - \frac{k_{\parallel}p_{\parallel}}{\gamma m_s} \qquad (2)$$

with $\omega_{RF}$ the frequency of the injected wave, $\ell$ the cyclotron harmonic number, $\Omega_s = q_s B / m_s c$ the cyclotron frequency for species $s$, $\gamma = 1/\sqrt{1 - v^2/c^2}$ the relativistic factor, $k_{\parallel}$ the wave vector parallel to the magnetic field, and $p_{\parallel} = \gamma m_s v_{\parallel}$ the particle momentum parallel to the magnetic field. Finally, $m_s$ and $q_s$ are the species rest

mass and charge respectively, and $c$ is the speed of light. If the value of $\mathbf{R}$ changes sign in one timestep, the particle has gone through resonance, and is therefore given a "kick" in energy.

The change in energy that the resonant particle receives is given by

$$\Delta\epsilon = \Big(\frac{dD_{\epsilon\epsilon}}{d\epsilon}\Big)\Delta t + (6D_{\epsilon\epsilon}\Delta t)^{1/2}R_N \tag{3}$$

where $\epsilon = \gamma m_s c^2 + q_s \Phi$ is the total particle energy an for electrostatic potential $\Phi$, $D_{\epsilon\epsilon}$ is the energy diffusion cofficient from the quasilinear diffusion equation. $\Delta t$ is the timestep and $R_N$ is a uniformly distributed random number in the range $[-1, 1]$. The energy diffusion coefficient is a specified function of the particle rest mass, charge, parallel velocity, magnetic moment, gyroradius, cyclotron frequency and the parallel and perpendicular wave vectors[1]. The derivative of the energy diffusion coefficient with respect to total energy may also be written as

$$\frac{dD_{\epsilon\epsilon}}{d\epsilon} = \frac{\partial D_{\epsilon\epsilon}}{\partial \epsilon} + \alpha\frac{\partial D_{\epsilon\epsilon}}{\partial \mu} \tag{4}$$

where $\alpha = (1 - k_\| v_\| / \omega_{RF})/B$ and the magnetic moment $\mu = \gamma^2 m_s v_\perp^2 / 2B$.

The first term on the right side of (3) represents the change in total energy due to dynamic friction or drag, while the second term represents the change due to diffusion in $\epsilon, \mu$ space. These are the same two processes that are described by the Fokker-Planck collision operator. Note that the energy increment $\Delta\epsilon$ may be either positive or negative, such that the particle gains energy from the wave, or vice versa, depending upon the direction of particle gyration.

Once the total energy increment is known, we calculate the change in the particle parallel momentum and magnetic moment by

$$\Delta p_{\parallel} = \gamma m_s c^2 \frac{k_{\parallel} v_{\parallel}}{\omega_{RF}} \frac{\Delta \epsilon}{p_{\parallel} c^2} \tag{5}$$

and

$$\Delta \mu = \frac{\gamma}{B}(1 - \frac{k_{\parallel} v_{\parallel}}{\omega_{RF}})\Delta \epsilon = \frac{\gamma}{B} \alpha \Delta \epsilon. \tag{6}$$

This implementation of the model was used earlier by Rognlien in the Monte Carlo RF-heated mirror code MCPAT[2,3].

## Simulation Results

In addition to the data required to run the basic electrostatic particle code, TESS also requires the following data for the RF heating model: the center and width of the RF heated region ($Z_{o_{RF}}$ and $\Delta Z_{RF}$), the wave frequency ($\omega_{RF}$), the cyclotron harmonic number of the wave ($\ell$), the peak RF wave amplitude ($E_{RF}(Z_{o_{RF}})$) and the parallel and perpendicular wave vectors ($k_{\parallel}$ and $k_{\perp}$).

Results of the TESS code are compared to those from MCPAT below. For these runs, the magnetic field profiles were specified in both codes, and the self-consistent calculation of the ambipolar electrostatic potential was disabled in TESS, in an effort to more closely compare with MCPAT, which does not have this capability. The runs are therefore simulations of a simple mirror geometry, with ECRH applied at the

bottom of the magnetic well. The RF waves are injected essentially perpendicular to the magnetic field at the bottom of the magnteic well, with a small component along the magnetic field. The input data for the runs were $Z_{o_{RF}} = 250$cm, $\Delta Z_{RF} = 50$cm. $\omega_{RF} = 8.8 \times 10^{10}$rad/sec, $E_{RF}(Z_{o_{RF}}) = 3$V/cm, $\ell = 1$ or fundamental heating. and $k_\perp = 1.0$cm$^{-1}$ and $k_\parallel = 0.1$cm$^{-1}$.

The electron velocity-space plots for the RF heated region from TESS and MC-PAT are shown in Figure 1 below. Note the increase in particle density in the regions of high $v_\perp$ and low $v_\parallel$, which is the indication of preferential heating in the $\perp$-direction. relative to the $\parallel$-direction. The initial thermal velocity in each direction is $v_{th} = 4.19 \times 10^8$cm/sec. such that the most energetic particles have been heated to a maximum velocity $v_{\perp_{max}} \simeq 6v_{th}$.

The kinetic energy profiles along the axis of the simple mirror are shown in Figure 2. Note that the TESS result is an instantaneous snapshot, while the MCPAT result is time-averaged. The MCPAT profile from $-150$cm to $150$cm corresponds to the region from 100 to 400cm (the peaks of the magnetic field) on the TESS profile. Note that in each case, the parallel kinetic energy is, on average. half that of the perpendicular kinetic energy. This is because the perpendicular direction comprises two degrees-of-freedom, as compared with one for the parallel direction. The heating is manifest almost entirely in the increase of the perpendicular kinetic energy in the 25cm to either side of the injection center point. TESS gives a maximum perpendicular kinetic energy of 215eV, while MCPAT yields a 200eV maximum
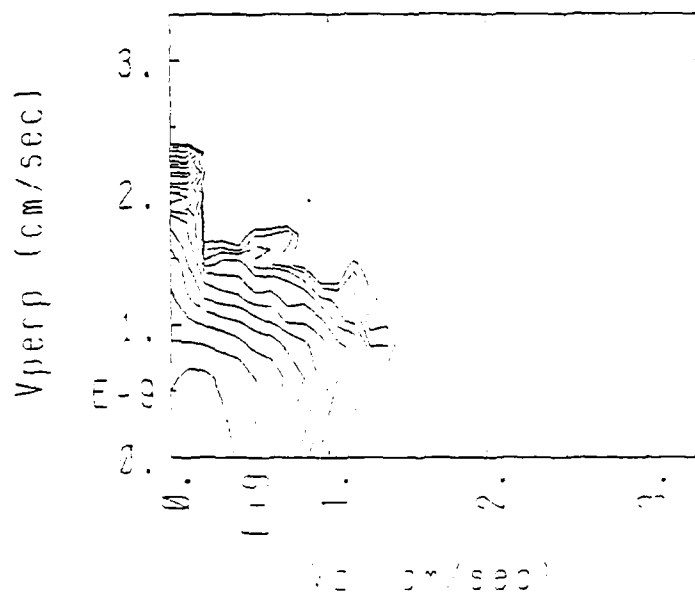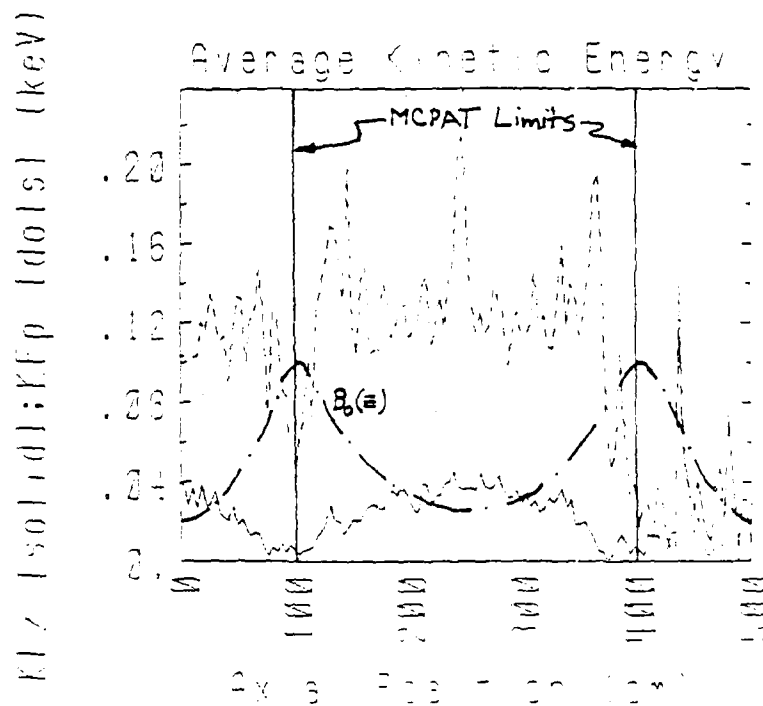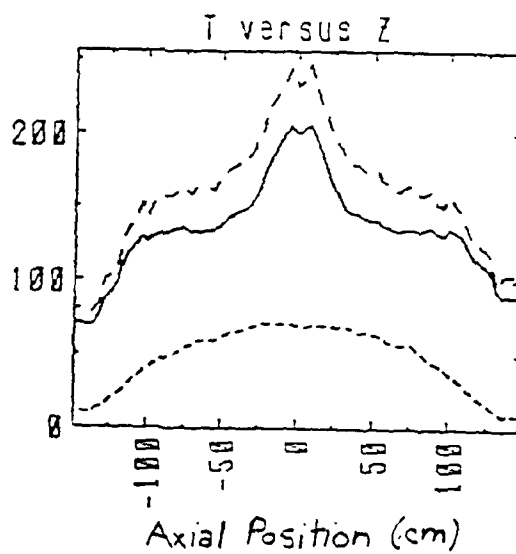
a) TESS velocity space density plot.



$V_z$ (cm/sec)
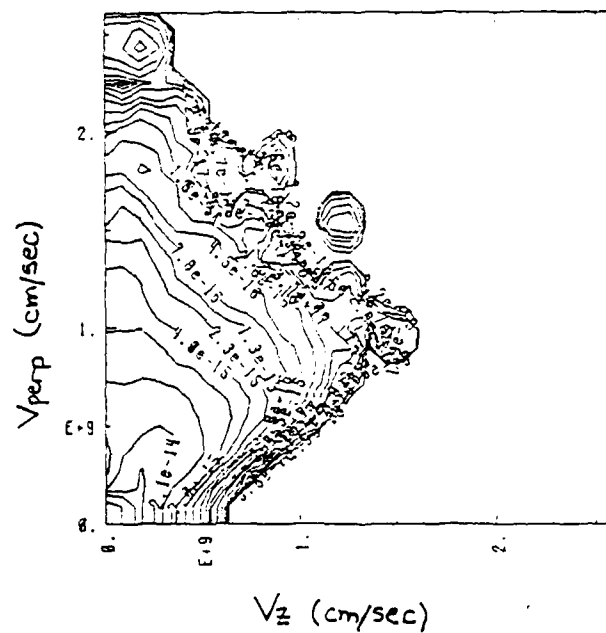
b) MCPAT velocity space density plot.

Figure 1. Electron $v_\perp$, $v_\parallel$ velocity space density plots for the region near the bottom of the magnetic well. showing the preferential increase in perpendicular velocity due to heating by applied electromagnetic waves.

a) Instantaneous kinetic energy profile from TESS.



b) Time-averaged kinetic energy profile from MCPAT.

Figure 2. Electron kinetic energy profiles showing the increase in perpendicular kinetic energy in the RF-heated region. The RF-heated region is 25cm on either side of the magnetic well minimum.

value. The large values of the perpendicular kinetic energy near the peaks of the magnetic field in the TESS results are due to particles which are near their turning points, with large values of $v_\perp$ and nearly zero values of $v_\parallel$. This effect is not seen in the MCPAT results due to the time-averaging of the profile.

The results from TESS compare favorably to those of MCPAT. The next step in this research with TESS is to calculate the electrostatic potential self-consistently. allow the particles to collide in addition to their diffusion due to the ECRH. and thereby determine the effect that RF-heating has on the overall particle confinement time. An additional area of research will entail a comparison of the results from TESS and a bounce-averaged Fokker-Planck code for the simulation of particle confinement in an RF-heated simple mirror. This comparison will be based upon velocity distribution function resolution, computational cost effectivness and ease of operation.

# References

[1]    I. B. Bernstein and D. C. Baxter, *Phys. Fluids.* **24**, 108 (1981).

[2]    T. D. Rognlien, *Phys. Fluids.* **26**, 1545 (1983).

[3]    T. D. Rognlien, *Nucl. Fusion*, **23**, 163 (1983).

# SECTION III: JOURNAL ARTICLES, REPORTS, TALKS, VISITS

## Journal Articles

K. Theilhaber, G. Laval, and D. Pesme, "Numerical simulations of turbulent trapping in the weak beam-plasma instability," Phys. Fluids, 30, pp. 3129-3149, October 1987.

K. Y. Kim, "Theory of Nonmonotonic Double Layers," Phys. Fluids 30, pp. 3686-3694, December 1987.

## Reports

William S. Lawson, "The Pierce Diode with an External Circuit. II. Non-uniform Equilibria," University of California, Berkeley, Memorandum No. UCB/ERL M87/52, July 1987.

Scott E. Parker, "Electrostatic Potential Formation Due to an Large Dip in the Magnetic Field with Application to FRC Confinement. University of California, Berkeley, Memorandum No. UCB/ERL M87/62, September 1987.

William S. Lawson, "The Pierce Diode with an External Circuit. III. Chaotic Behavior," University of California, Berkelely, Memorandum No. UCB/ERL M87/74, October 1987.

## Poster Papers/Talks

*Poster papers at 12th Conference on Numerical Simulation of Plasmas,* September 21-23, 1987, San Francisco, California:

A. Friedman, S.L. Ray, C.K. Birdsall, and S.E. Parker, "Particle-in-Cell Plasma Simulation with a Wide Range of Space and Time Scales."

S.E. Parker, "Numerical Error in Electron Orbits with Large $\omega_{c_e} dt$."

B.I. Cohen, J.C. Cummings, R.J. Procassini, and C.K. Birdsall, "Direct Implicit Particle Simulation of Mirror Transport."

W.S. Lawson and T.L. Crystal, "Artificial Cooling Due to Quiet Injection in Particle Simulation of a Bounded Plasma."

*Talks presented at US-Japan Workshop on Plasma Modeling with MHD and Particle Simulations,* September 25-26, 1987, Napa, California. (Professor C.K. Birdsall was host, USA organizer):

A. Friedman, C.K. Birdsall, S.E. Parker, S.L. Ray, "Multi-Scale Particle Simulations."

K.S. Theilhaber, C.K. Birdsall, "Observing Kelvin-Helmholtz Mode Growth Near a Wall, Producing Long-Lived Vortices, in a Magnetized Plasma."

*Invited talk at APS Division of Plasma Physics Twenty-Ninth Annual Meeting,* November 2-6, 1987, San Diego, California (abstract follows):

K. Theilhaber, "Vortex Formation and Transport to the Wall in a Crossed-Field Sheath."

*Poster Papers at APS Division of Plasma Physics Twenty-Ninth Annual Meeting*, November 2-6, 1987, San Diego, California (abstracts follow):

C. K. Birdsall, K. S. Theilhaber, and S. Kuhn, "Ion Acceleration in a Plasma Source Sheath."

A. Friedman, S. L. Ray, S. E. Parker and C. K. Birdsall, "Prospects for Multi-Scale Particle-in-Cell Simulation of Plasmas."

Wm. S. Lawson, "Investigations of the Pierce Diode Strange Attractor."

S. E. Parker, C.K. Birdsall, A. Friedman, and S. L. Ray, "Direct Implicit Particle Simulation of a Bounded Plasma System."

R. J. Procassini, J. C. Cummings, C. K. Birdsall, and B. I. Cohen, "Direct Implicit Particle Simulation of Simple Mirrors."

L. A. Schwager, "The Effect of Thermionic and Secondary Electron Emission at the Collector on Potential Drop and Transport Through the Plasma-Sheath Region."

**Vortex Formation and Transport to the Wall in a Crossed-Field Sheath\*.**

K. THEILHABER, ERL, University of California, Berkeley, CA 94720.

Particle simulations of a transversely magnetized sheath have been conducted with the aim of modeling plasma behavior in the vicinity of the limiters and walls of a fusion device. In the model the magnetic field is parallel to the wall. The two-dimensional, electrostatic, bounded particle simulation code ES2 has been used as a tool for the investigation of these edge effects. The simulations show that the bounded plasma is selfconsistently subject to a Kelvin-Helmholtz instability, which is driven by the non-uniform electric field created by the preferential charging of the boundries by ions. This instability is seen to evolve into many vortices which coalesce into large vortices ($e\psi/T_i\approx 1$) which drift parallel to the walls; these vortices convect particles to the walls at an anomalous rate much greater that that induced by collisional diffusion. Volume ionization of neutrals has been modeled by electron-ion pair creation; this results in a steady-state, in which the linear edge instability, the nonlinear fluid dynamics of the vortices, and the nonlinear dynamics of the particles scattered to the walls by the vortices all balance each other. This steady-state but non-equilibrium configuration can be likened to Rayleigh-Benard convection. Results will be presented for the scaling of transport as a function of the edge parameters, and for the characteristics of the spectrum of the E×B turbulence. A computer-generated movie wil be shown, illustrating vortex formation and coalescence in the sheath, and the resulting depletion of particles.

**Ion Acceleration in a Plasma Source Sheath.** C.K. BIRDSALL, K.S. THEILHABER, S. KUHN, ERL, Univ of Calif., Berkeley CA 94720 - A planar plasma source emitting warm electrons and cool ions may create a monotonically decreasing potential which repels some of the electrons and accelerates all of the ions, in a model which is the dual of the Bohm collector sheath. For cold ions and Boltzmann electrons, $\emptyset''=0(n_i=n_e)$ gives a maximum ion flux for a source sheath potential drop of $e\emptyset/kT_e=-0.5$, hence an ion velocity of sound speed. Next, invoking a real source field, $(E(0)^2>0)$, leads to a somewhat smaller maximum ion flux at $e\emptyset/kT_e=-1.256$, with ion speed of $1.585v_s$. Last, adding an initial ion velocity, we find analytic expressions for ion flux and plasma potential (measured at $\emptyset''=0$) which agree well with the numerical results of Kuhn (1) who used the proper cut-off Gaussians for both electron and ion velocity distributions. Thus, in a collisionless plasma, the Bohm "pre-collector-sheath" can be replaced by a planar source field (or by a distributed source) eliminating the need for postulating a pre-sheath acceleration by a small force acting over a long distance.
(1) S. Kuhn, Plasma Physics, Vol.23, p881, 1981; see Fig.2a.

**Prospects for Multi-Scale Particle-in-Cell Simulation of Plasmas.**[*] A. FRIEDMAN and S.L. RAY, *LLNL*, and S. PARKER and C.K. BIRDSALL, *U.C. Berkeley* — A long-standing goal in plasma simulation has been a method which could treat both detailed kinetic physics and smooth large-scale physics in an efficient and natural way. We describe a proposed technique[1] which would be suitable for strongly inhomogeneous problems involving a wide range of space and time scales, and the beginnings of our investigation into its feasibility. For such problems to be tractable, the particles in each part of phase space must be advanced on their own natural timescales, which are set by accuracy criteria (*e.g.*, limits on $\omega_{trap}\Delta t$ or $kv\Delta t$). In the past, this has been deemed impractical due to the requirement of a self-consistent field. We propose to overcome this difficulty by combining implicit PIC methods with a nonuniform mesh and suitable interpolations in time. Since most particles are not processed on any given step, on suitable problems we can hope for orders-of-magnitude speed improvements over explicit codes.

[1] A. Friedman, 2nd US-Japan Workshop on Advanced Plasma Modeling, Nagoya, March 1987.

**Investigations of the Pierce Diode Strange Attractor.**[*]
Wm.S. Lawson, *E.R.L., Univ. of Calif., Berkeley* — The strange attractor discovered by Godfrey[1] in the Pierce Diode system near $\alpha = 2.85\pi$ is studied. While the results differ slightly from those of Godfrey (his time step was not small enough for accurate convergence), the existence of the attractor is verified, and some other properties are noted. The changes in the attractor upon the introduction of a capacitor into the external circuit are also investigated. The results show that even a high capacitance (1000 times the vacuum capacitance of the diode itself) results in significant changes in the morphology of the attractor as a function of $\alpha$. Further reduction in the external capacitance shifts the position of the attractor slightly, and the amplitude of the electric field excursions doubles. By the time the external capacitance reaches five times the internal capacitance, the strange attractor has vanished.

[1] B.B. Godfrey, *Phys. Fluids* **30**(1987), 1553

**Direct Implicit Particle Simulation of a Bounded Plasma System.**[*] S.E. PARKER and C.K. BIRDSALL, *U.C. Berkeley,* and A. FRIEDMAN and S.L. RAY, *LLNL* — We are developing a direct implicit electrostatic particle code which models a one dimensional bounded system. The system has injection and absorption of plasma at the boundaries, with the left plane grounded and the right plane floating (open circuit). One objective is to use large $m_i/m_e$ and long time steps in order to obtain low frequency ion behavior in detail, including that at the source and collector sheaths. While the implicit method resolves long wavelengths well, there are questions about resolving the shorter wavelength behavior in the sheath regions. Hence comparison with results from an explicit one dimensional bounded code[1] will be presented. A long term goal will be to use this code as a test bed for particle simulation with variable space and time scales. A scheme has been proposed where particles will be moved at their respective time scales depending on their location in phase space[2].

[1] W.S. Lawson, "PDW1 User's Manual", ERL Report April 1984.
[2] A. Friedman, *et al*, APS-DPP, November 1987.

**Direct Implicit Particle Simulation of Simple Mirrors.**[*]

R. J. PROCASSINI, J. C. CUMMINGS and C. K. BIRDSALL, *University of California, Berkeley*, and B. I. COHEN, *Lawrence Livermore National Laboratory* — The simulation of particle confinement in a simple mirror plasma is possible with the one-dimensional (axial), relativistic, electrostatic particle code **TESS**. Our recent advances in the development of **TESS** include the addition of a quasilinear RF energy diffusion model for both ICRH and relativistic ECRH heating , and the addition of a neutral beam injection model which simulates plasma heating via charge exchange and impact ionization processes. The results of a self-consistent **TESS** simulation of particle confinement and transport in an auxiliary heated simple mirror plasma will be presented. These results will be compared to those from a Monte Carlo RF heating code and a Fokker-Planck code vis a vis velocity distribution function resolution, computational cost effectiveness and ease of operation.

**The Effect of Thermionic and Secondary Electron Emission at the Collector on Potential Drop and Transport Through the Plasma-Sheath Region.**[*] L. A. SCHWAGER, *U. C. Berkeley* — The region between a Maxwellian plasma source and an absorbing surface which emits thermionic or secondary electrons is modeled numerically with electrostatic particle simulation and analytically with a kinetic plasma-sheath equation. Results from these analytical and numerical models for collector potential and plasma transport show excellent agreement. Our energy transport results at critical emission (field reversal) and beyond compare well with such works as Hobbs and Wesson[1] who assume $\tau \ll 1$ (where $\tau = T_i/T_e$, the ion/electron source temperature ratio). Our potential drop across the collector sheath is slightly more negative (by 5% for $\tau = 0.1$ and by 12% for $\tau = 1$) than theirs. The plasma source, with a zero field boundary, emits equal fluxes of half-Maxwellian ions and electrons with specified mass and temperature ratios. The floating collector emits thermionic or secondary electrons, with temperatures of 1% $T_e$, which are accelerated into and interact with the plasma. Spatial profiles of potential and particle and energy fluxes are shown from simulation and compared with theory.

[1]G. D. Hobbs and J. A. Wesson, *Plasma Physics* 9, 85, (1967).

DISTRIBUTION LIST

**AFWL/DYP**
Pettus

**Department of Energy**
Crandall, Katz, Lankford, Macrusky, Manley,
Sadowski, Tech. Info. Center

**Department of Navy**
Condell, Florance, Roberson

**Argonne National Laboratory**
Brooks

**Austin Research Associates**
Drummond, Moore

**Bell Telephone Laboratories**
Hasegawa

**Berkeley Research Assoc.**
Brecht, Orens, Thomas

**Berkeley Scholars, In.**
Ambrosiano

**Cal. Inst. of Technology**
Bridges, Gould

**Calif. State Polytech. Univ.**
Rathmann

**Cambridge Research Labs.**
Rubin

**Columbia University**
Chu

**Cornell University**
Otani

**Dartmouth**
Hudson, Lotko

**E. P. R. I.**
Scott

**GA Technologies**
Bernard, Evans, Helton, Jee

**GTE Laboratories**
Rogoff, Winsor

**Hascomb Air Force Base**
Rubin

**Hewlett-Packard Laboratories**
Gleason, Marcoux

**Hughes Aircraft Co., Torrance**
Adler, Longo

**Hughes Research Lab., Malibu**
Harvey, Hyman, Poeschel, Schumacker

**Institute of Fusion Studies, Texas**
Librarian

**JAYCOR**
Klein, Tumolillo

**JPL**
Liewer

**Kaman Science Corp.**
Hobbs

**Lawrence Berkeley Laboratory**
Cooper, Kaufman, Kunkel,

**Lawrence Livermore National Lab.**
Albritton, Anderson, Barr, Brengle, Briggs,
Bruijnes, Byers, Chambers, Chen, B.Cohen, R.
Cohen, Denavit, Estabrook, Fawley, Fowler,
Friedman, Freis, Fuss, Harte, Hewett, Killeen,
Kruer, Langdon, Lasinski, Lee, Maron, Matsuda,
Max, Nevins, Nielsen, Smith, Tull, Ziolkowski

**Lockheed**
Siambis

**Los Alamos Scientific Lab.**
Barnes, Borovsky, Forslund, Kwan, Lindemuth,
Mason, Nielson, Oliphant, Peratt, Sgro, Thode

**Mass. Inst. of Technology**
Berman, Bers, Gerver, Lane, Palevsky

**Mission Research Corporation**
Godfrey, Mostrom

**Naval Research Laboratory**
Boris, Craig, Haber, Joyce, Orens, Roberson,
Vomvoridis

**New York University**
Lawson, Weitzner

**Northeastern University**
Chan, Silevitch

Oak Ridge National Lab.
Fusion Energy Library, Lebouef, Meier, Mook

Physics International
Woo

Princeton Plasma Physics Lab
Chen, Cheng, Lee, Okuda, Tang, Graydon,
Librarian

Lodestar Research Corp- Boulder
D'Ippolito, Myra

SAIC - Virginia
Drobot, Mankofsky, McBride, Smith

Sandia Labs, Albuquerque
Freeman, Poukey, Quintenz, Wright

Sandia Labs, Livermore
Marx, Wilson, Hsu

Stanford University
Blake, Buneman, Gledhill Physics Library,
Storey

TRW
Wagner

Vista Research Inc.
Crystal

University of Arizona
Carlile

University of California, Berkeley
Arons, Birdsall, Chorin, Graves, Cummings,
Haller, Hess, Lichtenberg, Lieberman, McKee,
Morey, Morse, Parker, Procassini, Roth,
Verboncoeur

University of California, Davis
DeGroot

University of California, Irvine
Rynn

University of California, Los Angeles
Abdou, Dawson, Decyk, Prinja

University of Illinois
Kushner

University of Iowa
Joyce, Knorr, Nicholson

University of Maryland
Guillory, Rowland, Winske

University of New Mexico
Anderson, Humphries

University of Pittsburgh
Zabusky

University of Southern California
Kuehl

University of Texas
Horton, McMahon, Tajima

University of Washington
Potter

University of Wisconsin
Emmert, Hershkovitz, Intrator, Shohet

Varian Associates
Anderson, Helmer

Universität Innsbruck
Cap, Kuhn

I.N.P.E.
Bittencourt, Montes

University of Toronto
Stangeby

Riso National Laboratories
Lynov, Pecseli

Culham Laboratory
Eastwood

Imperial College
Burger

Oxford University
Allen, Benjamin, Edgley

University of Reading
Hockney

Ecole Polytechnique, Palaiseau
Adam

Universite Paris
Raviart

IPP-KFA
Reiter

**Max Planck Institute für Plasmaphysik**
Biskamp, Chodura

**University Bayreuth**
Schamel

**Universität Kaiserslautern**
Wick

**Israel**
Gell

**Tel Aviv University**
Cuperman

**Hiroshima University**
Tanaka

**Kyoto University**
Abe, Matsumoto, Jimbo

**Nagoya University**
Kamimura, Research Info. Center

**Osaka University**
Mima, Nishihara

**Shizuoka University**
Saeki

**Tohoku University**
Sato

**University of Tromso**
Armstrong, Trulsen

**Centro de Electrodinàmica, Lisbon**
Brinca

**Ecole Polytechnique, Lausanne**
Hollenstein